Discover Nano

Research

Stigmurin encapsulated PLA–PEG ameliorates its therapeutic potential, antimicrobial and antiproliferative activities

Akshita Thakur[1] · Hema K. Alajangi[1,2] · Akanksha Sharma[1,2] · Euimin Hwang[3] · Akhil Khajuria[2] · Laxmi Kumari[2] · Pradeep Kumar Jaiswal[4] · Yong-beom Lim[3] · Gurpal Singh[2] · Ravi Pratap Barnwal[1]

Received: 26 October 2024 / Accepted: 25 February 2025
Published online: 10 March 2025

Abstract

In light of growing global challenge posed by antimicrobial resistance, it is very important to explore alternatives that can target pathogenic microorganisms. One such strategy involves the use of antimicrobial peptides (AMPs) and Stigmurin is one such AMP present in Brazilian scorpion *Tityus stigmurus* which possesses antimicrobial, antiproliferative and antiparasitic activity. The study commenced with successful synthesis and characterization of Stigmurin and its analogues, designated S1 and S2. Studies on Stigmurin and its analogues have demonstrated that analogues exhibit enhanced antimicrobial efficacy but often lead to increased hemolysis, limiting their therapeutic application. To prevent the associated toxicity of these peptides, PLA–PEG di-block copolymer was synthesised to prepare nanoparticles (E-WT, E1, and E2) with an average diameter of approximately 160–180 nm. The core of the research involved evaluating the antimicrobial (*Bacillus subtilis*), antibiofilm (*B. subtilis* and *Pseudomonas aeruginosa*), antiproliferative (HEK293 and RAW264.7) and hemolytic activity of the peptides. In addition to the experimental work, in silico analysis using structural models was conducted to further understand their potential interactions. The findings demonstrated that the analogue peptides exhibit enhanced antimicrobial and antibiofilm activity compared to the wild-type Stigmurin. Moreover, encapsulating the peptides in PLA–PEG nanoparticles maintained the antimicrobial activity against *B. subtilis*. Further, encapsulation significantly reduced hemolysis as well as cytotoxicity by 10–20%, thereby improving their safety profile.

Highlights

1. PLA–PEG encapsulation of Stigmurin and its analogue peptides were undertaken.
2. In silico binding evaluation of these peptides against *Bacillus subtilis* and *Pseudomonas aeruginosa*, responsible for biofilm formation, was done.
3. In vitro studies revealed that Stigmurin analogues exhibit potent antimicrobial activity against *B. subtilis* as well as antiproliferative activity.
4. Encapsulation of the analogues reduced hemolysis and cytotoxicity for their safer delivery.

Akshita Thakur, Hema K. Alajangi and Akanksha Sharma equal contributions.

Supplementary Information The online version contains supplementary material available at https://doi.org/10.1186/s11671-025-04224-8.

✉ Yong-beom Lim, yblim@yonsei.ac.kr; ✉ Gurpal Singh, gurpalsingh.ips@gmail.com; ✉ Ravi Pratap Barnwal, barnwal@pu.ac.in | [1]Department of Biophysics, Panjab University, Chandigarh 160014, India. [2]University Institute of Pharmaceutical Sciences, Panjab University, Chandigarh 160014, India. [3]Department of Materials Science and Engineering, Yonsei University, Seoul 03722, Korea. [4]Department of Biochemistry and Biophysics, Texas A & M University, College Station, TX 77843, USA.

Keywords Stigmurin · Analogues · PLA–PEG · Encapsulation · Antimicrobial peptide · Nanotechnology

Abbreviations

AMPs	Antimicrobial peptides
PLA	Polylactic acid
PEG	Polyethylene glycol
MIC	Minimum inhibitory concentration
MBC	Minimum bactericidal concentration
DMEM	Dulbecco's Modified Eagle Medium
FBS	Fetal bovine serum
HEK	Human embryonic kidney cells
RPMI1640	Roswell Park Memorial Institute
MTT	3-(4,5-Dimethylthiazol-2-yl)-2,5-diphenyltetrazolium bromide) tetrazolium

1 Introduction

Antimicrobial peptides (AMPs) exhibit an expansive spectrum of activity against microbes in a wide range of organisms [1, 2]. AMPs are generally positively charged and comprised of short chains of amino acids predominantly composed of hydrophobic residues that weigh less than 9 kDa. [3]. AMPs have earned the nickname of "new age antibiotics" due to their distinct mechanism of action, being potential alternatives to conventional antibiotics. Microorganisms can develop resistance to antibiotics over time, rendering them ineffective, whereas AMPs often work through multiple mechanisms, making it harder for microbes to develop resistance and thus making them potentially more sustainable in the long run [4–6]. AMPs typically act quickly, often by disrupting cell membranes or inhibiting vital processes in microorganisms [7].

AMPs are naturally produced by virtually all organisms: plants, insects and animals, which form the basis of their innate immunity defence. Venomous animals are a rich source of AMPs, for example, melittin is the primary AMP found in bee venom and has very strong antimicrobial and anticancer activities [8]. Scorpion venom is comprised of a complex mixture of biologically active constituents for various purposes, and among these components are AMPs, which play a defensive role against infections [9]. In 2015, De Melo et al. discovered Stigmurin, a specific AMP comprised of 17 residues (FFSLIPSLVGGLISAFK-NH_2) (net charge + 1), within the venom gland of brazilian scorpion *Tityus stigmurus* [10]. It may exhibit its antimicrobial effects through membrane disruption [10]. The cationic and amphipathic nature can facilitate the interaction with negatively charged bacterial membranes, leading to increased permeability and cell lysis.

To improve the antimicrobial action, *Parente* et al. further modified Stigmurin to create two analogous peptides, S1 (FFSLIPKLVKGLISAFK-NH2) and S2 (FFKLIPKLVKGLISAFK-NH2) [11]. This was achieved by replacing glycine and serine residues with lysine, resulting in increased net charge of + 3 and + 4 for S1 and S2, respectively. Furthermore, the hydrophobic moment of the peptides also increased, measuring 0.669 for S1 and 0.725 for S2 [12]. Stigmurin and its analogues (S1 and S2) exhibit antimicrobial activity in vitro and in vivo along with antifungal, anti-parasitic activity and anti-proliferative effects on the HeLa cell line [13, 14]. Notably, analogue peptides S1 and S2 show enhanced antimicrobial activity within 1–25 µM concentration range, specifically targeting Gram-positive bacteria. However, it is important to highlight that these peptides also cause increased hemolysis in human erythrocytes, inducing 30% hemolysis at a concentration of 75 µM [12].

Studies on Stigmurin and its analogues have demonstrated that modifications to enhance antimicrobial efficacy often led to increased hemolytic activity, limiting their therapeutic application as free peptides. Another study including analogues such as StigA25 and StigA31 exhibited potent antimicrobial activity, with minimum inhibitory concentrations (MICs) lower than 4.7 µM and 2.3 µM, respectively, in Gram-positive bacteria. However, these analogues also showed concentration-dependent hemolytic activity, with significant hemolysis observed at higher concentrations [13]

The increased hemolytic activity underscores a limitation in the direct application of AMPs. To address this challenge, our study employed PLA–PEG encapsulation of these peptides. Some studies have shown the potential of polymer-based delivery systems in reducing the toxicity of AMPs while maintaining or enhancing their antimicrobial activity. For instance, the use of DSPE-PEG2000 micelles has been shown to improve the hemolytic activity and cytotoxicity profiles of AMPs, making them more suitable for therapeutic applications [15, 16]

Polylactic acid (PLA) is a synthetic polymer known for its biodegradability, low immunogenicity and robust mechanical properties [17]. In contrast, polyethylene glycol (PEG) possesses excellent hydrophilicity, flexibility and biocompatibility. PLA–PEG copolymeric system offers several advantages for delivering AMPs compared to other polymeric systems. Combining the biodegradability and mechanical strength of polylactic acid (PLA) with the hydrophilicity and biocompatibility of polyethylene glycol (PEG), PLA–PEG copolymers form nanoparticles that degrade into non-toxic byproducts, such as lactic acid and water, making them suitable for drug delivery applications [18] This system enhances AMP stability and reduces aggregation, outperforming more hydrophobic polymers like poly(lactic-co-glycolic acid) (PLGA) [19, 20]. Additionally, the amphiphilic nature of PLA–PEG allows for controlled and sustained release of AMPs, minimizing rapid degradation or clearance [21]. Furthermore, the properties of the copolymer can be tailored by adjusting the PEG-to-PLA ratio, enabling precise control over release rates and degradation profiles, which is advantageous over other carriers such as chitosan or lipid-based systems [22] Peptide-loaded nanoparticles interact with various cells differently, in cancer cells, cationic AMP interact with the phospholipids efficiently. On the other hand, healthy cells resist interaction due to neutral membranes, and bacterial membrane resist due to the presence of anionic phospholipids as shown in Fig. 1.

The objective of the study was to investigate and compare antibacterial activity of the stigmurin peptide as well as its analogues S1 and S2 with and without encapsulation with PLA–PEG copolymer. Additionally, the mechanism of action of AMP was established via in silico approaches. To investigate the impact of encapsulation, antimicrobial, antibiofilm, cytotoxicity and hemolytic assays were conducted. The antimicrobial assay compared the antimicrobial activity of free and encapsulated peptides. The cytotoxicity assay assessed the cytotoxic effects of the peptides, while the hemolytic assay evaluated their respective hemolytic effects. Results indicated that encapsulation significantly improved cell viability and reduced erythrocyte hemolysis.

In this study, structural models of peptides Stigmurin (S-WT), S1 and S2 were generated, and molecular docking was performed with bacterial proteins using HADDOCK platform. Further, molecular dynamics (MD) simulations were performed for the best protein-peptide complex to determine the overall stability. Following this, nanoparticles were synthesized, antimicrobial activity of the free peptides and encapsulated peptides was observed against *Bacillus subtilis.* Antimicrobial

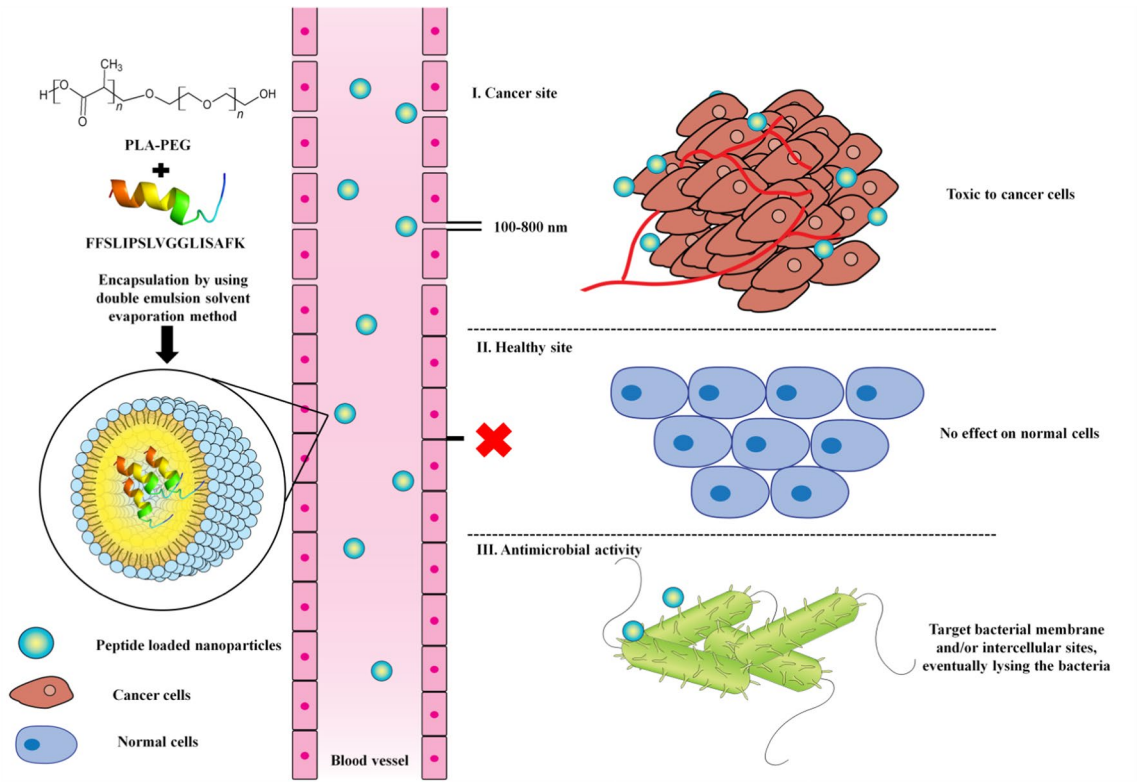

Fig. 1 Peptide loaded nanoparticles **I** Plasma membrane in cancer cells loses the natural phospholipid asymmetry, hence negatively charged surface of cancer cell interacts with cationic AMPs. **II** Normal cells in a healthy human host have low susceptibility to the AMPs due to the presence of neutral/zwitterionic membrane, therefore preventing the interaction with the AMPs and **III** Anionic phospholipids in the bacterial membrane favour the interaction with the AMPs

activity was evaluated by Mueller Hinton broth assay and minimum inhibitory concentration (MIC) and Minimum bactericidal concentration (MBC) values were determined against *Bacillus subtilis*. Additionally, the anti-biofilm activity of the peptides against *Pseudomonas aeruginosa* and *Bacillus subtilis* were determined by static anti-biofilm assay. The cytotoxicity activity of the peptides was assessed with RAW264.7 cells and HEK293 cells and finally, the hemolytic potential of the peptides was checked in human erythrocytes.

2 Methods and materials

2.1 Bacterial strains and chemicals

Strains of *Bacillus subtilis* MTCC 121 and *Pseudomonas aeruginosa* were a kind gift from the Department of Microbiology, Panjab University, Chandigarh; poly-lactic acid (PLA) particles, PEG-6000, Mueller Hinton Broth, microtiter plates (Polystyrene), Petri Plates, Nutrient Broth, Phosphate buffer (10x), Triton-X 100, ethanol, solvents including Polyvinyl alcohol (PVA), dichloromethane (DCM), dicyclohexylcarbodiImide (DCC), 4-dimethylaminopyridine (DMAP), 3-(4,5-dimethylthiazol-2-yl)-2,5-diphenyltetrazolium bromide (MTT) were purchased from Sigma–Aldrich Pvt. Ltd., India.

2.2 Synthesis of PLA–PEG copolymer and its characterization studies

A copolymer of PLA–PEG was prepared by using two components: polylactic acid (molecular weight of 72 kDa) and polyethylene glycol (PEG) (molecular weight of 6 kDa) via a previously reported method by Kumar et al.[23]. To achieve this, equal quantities of PLA (1.008 g, equivalent to 0.014 mmol) and PEG (0.084 g, equivalent to 0.014 mmol) were dissolved in 100 mL of dichloromethane (DCM) with continuous stirring at temperatures between 0 and 2 °C. Subsequently, 0.05 g of N, N-dicyclohexylcarbodiimide (DCC) was introduced slowly into the solution using a syringe. Following this, 2 mg of 4-dimethylaminopyridine (DMAP) was added to the solution, as depicted in Fig. 2. DCC and DMAP were used to couple the carboxyl and hydroxyl groups of PLA and PEG. The mixture was then allowed to stir for 16 h on a magnetic stirrer at 200 rpm. Any remaining polymer was removed using a mixture of methanol and diethyl ether in a 1:1 ratio. The resultant copolymer was then freeze-dried and subsequently stored at − 20 °C. The polymer structure was characterized using Fourier transform infrared spectroscopy (FT-IR) (PerkinElmer, Massachusetts, USA) and using proton nuclear magnetic resonance spectroscopy (^{1}H NMR) in $CDCl_3$ at 400 MHz (Bruker, Avance 400, Munich, Germany).

2.3 Preparation of nanoparticles

Peptides were encapsulated with PLA–PEG copolymer using double emulsion solvent evaporation method (w/o/w) with some modification [24]. Briefly, peptide suspension (1 mg/ml) was added to a co-polymeric solution (10 mg) dissolved in acetonitrile (5 ml) using vortex to form water-in-oil (w/o) emulsion. The emulsion was then sonicated using a 120 Sonic Dismembrator (Cole Parmer, USA) with a 3 mm probe for 60 s. The resulting water-in-oil (w/o) emulsion was then dropwise injected via a syringe in 1.5% w/v polyvinyl alcohol (PVA) via vortex to create a secondary emulsion and stirred using a magnetic stirrer at room temperature till the organic solvent completely evaporated. Nanoparticles were collected by centrifugation at 30,000 × *g* for 30 min. The resulting particles were washed twice using distilled water and resuspended in the same. The supernatant and washing solutions were collected and combined for spectrophotometric analysis to quantify the amount of non-entrapped drug. Washed nanoparticles were freeze-dried and stored at −20 °C for future use.

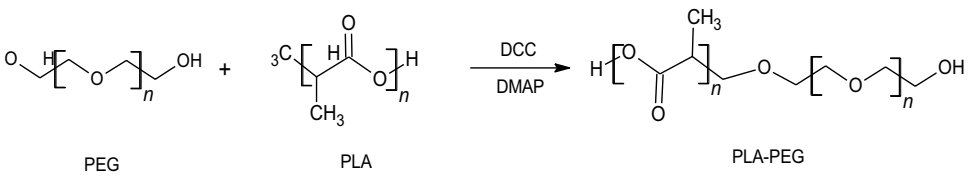

Fig. 2 PLA–PEG diblock copolymer prepared by using PLA and PEG in the presence of DCC and DMAP

2.4 Characterisation of nanoparticles

2.4.1 Particle size

Dynamic light scattering (DLS) is a hydrodynamic technique that measures the translational diffusion coefficients of particles, providing insights into their size and shape based on theoretical relationships. This method analyzes fluctuations in light scattering intensity caused by the Brownian motion of colloidal particles in suspension. As particles undergo random motion due to collisions with solvent molecules, the scattered light intensity varies accordingly. In this study, the mean particle size of AMP-loaded PLA–PEG nanoparticles was determined using DLS at 25 °C with a scattering angle of 90°. Freshly prepared nanoparticle dispersions were diluted 100-fold with distilled water, and measurements were conducted in triplicate. The average particle size was reported as the volume mean diameter, expressed as mean ± standard deviation (n = 3) [25].

The size and morphology of PLA–PEG polymeric nanoparticles were analyzed using a Hitachi SU8010 Series Field Emission Scanning Electron Microscope (FESEM), Japan. A small amount of freeze-dried nanoparticles was suspended in distilled water with sonication and vortexing and dried at room temperature on top of a carbon conductive tab held on top of an aluminium sample disk. SEM samples were sputter coated with metal plasma and images were obtained [26, 27]

2.4.2 Zeta potential and polydispersity index (PDI)

Zeta potential and PDI values were measured utilizing DLS, employing a Particle Analyzer (Delsa™ nano, Beckman Coulter, USA) at 25 °C and a scattering angle of 90°. To perform the measurements, the newly prepared nanoparticle dispersion was diluted 100 times with distilled water. All measurements were done in triplicate for accuracy. PDI values higher than 0.7 indicate that the sample has a very broad particle size distribution and is probably not suitable to be analysed by DLS technique [28].

2.4.3 FTIR spectra

FTIR spectroscopic analysis provides information on chemical bonding, functional groups and presence or absence of changes in the crystalline structure of a compound. Spectra obtained using infrared spectroscopy allows to determine physical and chemical properties of the material by recording frequency of vibrations that correlate with common atomic bonds. FTIR spectra for free peptides and peptide-loaded PLA–PEG nanoparticles were obtained using a PerkinElmer FTIR spectrometer (Massachusetts, USA) across a scanning range of 4000–500 cm^{-1}. Sample preparation involved thoroughly mixing the sample with potassium bromide (KBr) in a 1:10 ratio (sample:KBr) and compressing the mixture under a pressure of 160 Kpa [29].

2.4.4 Encapsulation efficiency

The efficiency was determined using a modified method since the peptides lack tyrosine, tryptophan and phenylalanine residues. Nanoparticles were centrifuged at 9000 rpm for 30 min to separate them from the dispersion. The supernatant was collected and diluted to analyze the amount of free peptide by using Nanodrop instrument (Thermo Fisher, USA) at a wavelength of 205 nm. [30] The percentage entrapment efficiency was then calculated as follows:

$$EE\% = \text{Total amount of peptide added}-\text{Free peptide}/\text{Total amount of peptide} * 100$$

2.5 In silico analysis

In silico approaches provide preliminary information, however, experimental investigation often helps reveal the precise mechanism of action. In other words, initial stage screening can be performed by in silico methods. Following this,

outcomes of in silico study would pave way for in vitro studies to ascertain the antimicrobial potential of stigmurin and its analogues S1 and S2.

2.5.1 Structure prediction

The freely available Google ColabFold notebook [31] was used to develop the structural model of peptides S-WT, S1 and S2. The notebook was slightly modified from the previous report of Deepmind's original notebook [32]. The input file for generating structural models includes the primary peptide sequence and sequence alignment [33]. The Amber-relaxation option was used to optimize side-chain bond geometry [34]. Structure models were visualized either in PyMOL (https://pymol.org/) or Chimera (https://www.cgl.ucsf.edu/chimerax/) [35].

2.5.2 Molecular docking

To investigate the interaction between the peptides (S-WT, S1 and S2) with bacterial proteins involved in biofilm formation, molecular docking was performed. Protein-peptide docking was performed using the High Ambiguity Driven protein–protein Docking (HADDOCK) (version 2.4) [36] molecular docking platform to calculate the models of the peptide (S-WT, S1 and S2) and the receptor protein complex. HADDOCK utilizes experimental data for molecular docking, unlike other docking protocols that rely only on structural coordinates. The docking process via HADDOCK involves randomization of orientations and energy minimization, torsion angle dynamics, and refinement with a solvent. PDB files were uploaded on the server and blind docking in ab-initio mode was performed. The "active" residues, as well as "passive" residues, were automatically defined. All the default parameters were considered for docking, except that in sampling parameters, the number of structures for rigid body docking was set to 10,000, number of structures for semi-flexible refinement was set to 400 and number of structures for final refinement was also set to 400. The clusters, ranked on the basis of HADDOCK score were checked for various interactions using LIGPLOT + software [37] (https://www.ebi.ac.uk/thornton-srv/software/LigPlus/). It generates a diagram of protein–protein interaction for the provided PDB file. Information on various parameters such as HADDOCK score, z-score, van der Waals energy, electrostatic energy, desolvation energy, etc. can be obtained on performing docking via HADDOCK. Further, binding affinity as well as total energy can be determined using the following equations [38]:

$$\text{Binding affinity} = \text{Haddock score} - (0.1 \times \text{restraint energy})$$

$$\text{Total energy(kcal/mol)} = \text{Van der Waals energy} + \text{electrostatic energy} + \text{desolvation energy}$$

To perform docking, Stigmurin peptides S-WT, S1, and S2 were selected, with their structures modelled with the help of AlphaFold [39]. TasA protein (PDB: 5OF1) in *B. subtilis* and Lectin LecA (PDB: 4LKD) in *P. aeruginosa* are biofilm forming proteins, so these proteins were chosen as receptor proteins for the work. TasA is the significant component of *B. subtilis* biofilm along with the exopolysaccharides [40]. Lectin LecA is crucial for biofilm formation and tissue attachment in *P. aeruginosa* [41].

2.6 Molecular dynamics simulations

To understand the conformational dynamics of the protein–ligand complex exhibiting good binding via molecular docking, we performed MD simulations. MD simulations were performed for the protein receptors TasA and Lectin LecA, S2 peptide as well as the protein-peptide complexes (TasA-S2 complex and Lectin LecA-S2 complex). Among all the peptides, S2 peptide exhibits best binding, therefore, its complex with the target proteins was chosen for MD simulations. Simulations were carried out for 100 ns duration on the SiBiolead server [42]. The optimized potentials for liquid simulations (OPLS/AA) force field were chosen for generating molecular topology. Additionally, a simple point charge (SPC) water model was used for filling the triclinic box. To neutralize the system, Na^+ and Cl^- ions were added. Energy minimization was performed for 5000 steps, with Steepest Descent integrator. The system was further simulated using NVT/NPT (isothermal-isobaric) ensemble. Modified Berendsen thermostat was used for NVT equilibrium, while Parrinello-Rahman barostat was used for NPT equilibrium. The simulation was performed at 300 K temperature and pressure equal to 1 bar [43, 44]Parameters like root mean square deviation (RMSD), root mean square fluctuation (RMSF) and radius of gyration (Rg) are used to analyze the data. RMSD estimates the differences in structure and dynamics of macromolecules and

determines the quality of biomolecular simulations. RMSF provides information about the relative fluctuations of every residue. To determine rigid and flexible regions, the flexibility of individual residues of the docked complexes is determined. On the other hand, the radius of gyration provides information about the compactness of the structure. Further, solvent-accessible surface area (SASA) plots were also generated. SASA refers to the exposed area of the protein which allows it to interact with solvent molecules. SASA is a crucial factor for determining protein function and stability [45].

2.7 Antimicrobial activity of Stigmurin and its analogues

MIC and MBC values were determined to assess the antimicrobial activity of the free and encapsulated peptides. MBC values were only defined for the analogues, whereas MIC values were determined for free and encapsulated peptides.

2.7.1 Minimum inhibitory concentration (MIC) assay

MIC is the lowest concentration of an antimicrobial agent that inhibits visible bacterial growth after incubation. MIC assay was performed following the Clinical and Laboratory Standards Institute (CLSI) guidelines using the flat-bottom 96-well microtiter plates [46]. The peptides were serially diluted in Mueller–Hinton broth (MHB) and 50 µl of each dilution was added to replicate wells in a plate. The Gram-positive bacterium *Bacillus subtilis* (MTCC 121) was used for antimicrobial assays. Bacteria cultured in MHB were diluted to 1×10^5 colony forming unit per ml (CFU/mL) in MHB. Subsequently, 50 µl of this bacterial suspension were added in triplicate to wells containing varying concentrations of AMPs ranging from 0.875 to 56 µM. The solutions were then incubated at 37 °C for 24 h, and microbial growth was assessed at 595 nm in a microplate reader. The sterility control (sterile MHB, 100 µl) and growth control (inoculum (50 µl) + sterile MHB (50 µl) to check sterility and to monitor normal bacterial growth, respectively, were also observed under the same conditions. The lowest concentration capable of preventing bacterial growth is the MIC value. These experiments were carried out in triplicate.

2.7.2 Minimum bactericidal concentration (MBC) assay

MBC values for the analogue peptides were determined using the method described by Al-Ani et al. [47]. The minimum bactericidal concentration (MBC) is defined as the lowest concentration of an antimicrobial agent that kills the bacteria. This concentration results in a substantial 3-logarithmic reduction in the size of the standard inoculum, indicating a 99.9% reduction in bacterial viability. Antimicrobial agents are considered bactericidal when their MBC value is less than four times the MIC. MBC was determined by evaluating bacterial growth at peptide concentrations of MIC, 2MIC, 4MIC, 6MIC and 8MIC. Following the same initial steps as the MIC assay., the dilutions were sub-cultured into Mueller–Hinton Agar (MHA) plates to determine the MBC. After 24 h incubation at 37 °C, colonies were observed and MBC was defined as the concentration at which no visible colonies were observed. [31].

2.8 Hemolytic assay

It is a method used to measure the release of hemoglobin into plasma as an indicator of red blood cell breakdown. Human B + erythrocytes were collected from blood sample of a healthy donor (Ethical clearance: PGI/IEC/2022/000734) for which informed consent as well as approval via ethical committee were obtained prior to the experiment. The erythrocytes were isolated by centrifugation at 2000 rpm for 10 min in a phosphate-buffered saline (PBS) solution (comprising 8.5 g NaCl, 0.4 g NaH_2PO_4, and 2.2 g Na_2HPO_4 per litre, with a pH of 7.4). Subsequently, the RBCs underwent three rounds of washing with PBS. A 2% vol/vol suspension of RBCs in PBS was then prepared and stored at 4 °C. For the assay, 50 µL of this suspension was mixed with 50 µL of peptides that had been serially diluted, ranging from 0.875 to 56 µM. In the positive control groups, 2% (v/v) Triton X-100 was added to the RBC suspension to induce 100% hemolysis. In contrast, for the negative control group, sterile PBS was added in combination with the RBC suspension for 0% hemolysis. The suspensions were incubated for 1 h at 37 °C and later centrifuged for 5 min at 2200 rpm. The resulting supernatant was transferred to a 96-well microtiter plate, and its optical density (O.D.) was measured at 540 nm using a microplate reader. The assays was performed in triplicate for each peptide concentration [48]. To determine the percentage of hemolysis caused by the peptides, the following equation was applied:

$$\text{Percentage (\%)hemolysis} = \frac{\text{O.D of test Concentration} - \text{O.D of negative control}}{O.D\ of\ positive\ control - O.D.\ of\ negative\ control}$$

2.9 Static biofilm assay

To perform static biofilm assay, *Bacillus subtilis* and *Pseudomonas aeruginosa* were grown overnight and adjusted to McFarland standards of 10^8 CFU/mL. Following this, the culture underwent an approximate 20-fold dilution in fresh nutrient broth to achieve the desired cell density, often aiming for an initial inoculum of 10^5 CFU/mL. Next, 200 µL of the prepared dilution was dispensed into a polystyrene plate (TPP® 96-well) and allowed to incubate at 37 °C for a duration of 20–24 h, with no agitation. Free peptides (S-WT, S1, and S2), encapsulated peptides (E-WT, E1, and E2), and PLA–PEG were added into the diluted bacterial culture with concentrations ranging between 1 and 1000 µM. The assay was performed in triplicates. The optical density (O.D.) of the suspended bacterial culture was assessed after incubation using a microplate reader (Synergy, USA) at 595 nm. The suspended cells were then discarded, and the plate was rinsed with 1 × phosphate-buffered saline (PBS) for removal of the suspended bacterial cells. Further, the sessile biofilm cells were stained with 1.0% crystal violet (1% crystal violet prepared in 20% methanol) solution for 30 min. This was followed by rinsing the plate with autoclaved water to remove unbound dye. The cells stained with the dye were then eluted with 100% ethanol, and further quantification was done by measuring O.D. at 545 nm. Biofilm was quantified by dividing the quantity of crystal violet bound to the biofilm (O.D. at 545 nm) by the number of suspended cells (O.D. 595 nm) [49].

2.9.1 Cytotoxicity activity

To assess the cytotoxic activity of S-WT, S1, S2 (free peptides) and EWT, E1, E2 (encapsulated peptides), 3-(4,5-dimethylthiazol-2-yl)-2,5-diphenyltetrazolium bromide tetrazolium reduction assay (MTT assay) was performed [50] The colorimetric assay involves the reduction of MTT, initially a yellow reagent, to form insoluble purple-colored formazan crystals. This transformation occurs because of the metabolic activity of the viable cells. HEK 293 and RAW 264.7 cells were cultured in Roswell Park Memorial Institute Medium (RPMI) 1640 Medium (Himedia) and Dulbecco's Modified Eagle Medium (DMEM) (Himedia) respectively, ensuring healthy, logarithmically growing cells. The cells were procured from NCCS, Pune, India. The medium was supplemented with 1% penicillin–streptomycin antibiotic solution (10,000 units/ml from Himedia) and 10% fetal bovine serum (FBS). The culture environment was maintained at 37 °C with 5% CO_2 within a CO_2 incubator (Eppendorf India Pvt. Ltd.). RAW 264.7 and HEK 293 cells were subjected to trypsinization and seeded into 96-well plates at a density ranging from 1 to 1.5×10^4 cells per well, with each well containing 200 µL of complete medium in an incubator. Following an initial incubation period, the cells were mixed with peptides at various concentrations, specifically serially diluted concentrations of 2 µM, 4 µM, 10 µM and 20 µM per well. This treatment was continued for an additional 24 h. On the subsequent day, 20 µL of reconstituted MTT solution, prepared in PBS, was introduced in each well and allowed to incubate for 4 h. After incubation, the supernatant was discarded, and 100 µL of DMSO was dispensed in each well to dissolve the purple formazan crystals. Color development was monitored as formazan crystals dissolved, with intermittent shaking to ensure thorough solubilization. The readings were measured in a microplate reader at 590 nm. Untreated cells, considered as control with 100% viability, served as the baseline for assessing relative cell viability in the test wells. The MTT assay was performed in triplicate.

$$Percentage\ cell\ viability = \frac{O.D\ of\ sample - O.D\ of\ blank}{O.D\ of\ control - O.D\ of\ blank} \times 100$$

2.9.2 Statistical analysis

To interpret the bioassays, multiple group comparisons were conducted using analysis of variance (ANOVA) with GraphPad Prism software (Version 5.00, GraphPad, San Diego, CA, USA). Bonferroni's multiple comparisons test was employed to calculate the confidence intervals and adjusted *p*-values.

3 Results and discussion

3.1 Synthesis and characterization of PLA–PEG polymer

The successful synthesis of PLA–PEG di-block copolymer is strongly supported by the observed chemical shifts in the proton NMR spectrum. The peak at 5.1 ppm corresponds to the methine protons (-CH) in the polylactic acid (PLA) backbone, while the peak at 1.6 ppm is attributed to the methyl ($-CH_3$) protons of PLA. The peak at 3.6 ppm is attributed to methylene (CH_2) protons of PEG (Supplementary Fig. 1). These characteristic peaks are consistent with previous studies that describe similar NMR spectral data for PLA–PEG block copolymers, confirming the structural integrity of the polymer [51, 52]. Furthermore, the FTIR spectra provide complementary evidence of the successful copolymer formation. The distinctive absorption bands for the ester carbonyl group (C=O) around 1750 cm^{-1} (from PLA) and the ether bonds (C–O–C) around 1100 cm^{-1} (from PEG) validate the polymer composition, which aligns with the literature on the synthesis of PLA–PEG copolymers (Supplementary Fig. 2) [53]. These findings corroborate that the coupling reaction mediated by DCC and DMAP has proceeded as expected, yielding the desired copolymer structure. In line with previous research, the amphiphilic nature of the PLA–PEG block copolymer facilitates micelle formation in aqueous environments. The hydrophobic PLA core and hydropilic PEG shell structure have been extensively characterized for their potential in drug delivery systems due to their ability to form stable micellar structures.

3.2 Synthesis and characterization of nanoparticles

PLA–PEG polymer based-nanoparticles were synthesized by a method commonly used for peptide encapsulation, i.e., double emulsion solvent evaporation. Earlier studies have shown that nanoparticles synthesized by the emulsification method require a stabilizer, such as PVA in the outer aqueous phase that functions as an emulsifier. It helps to maintain the secondary emulsion and droplets created by sonication, resulting in comparatively smaller and uniformly sized particles. Without the presence of PVA, emulsion droplets would amalgamate, preventing the formation of nanoparticles. PVA is reportedly carcinogenic and inhibits the uptake of nanoparticles by cells. Moreover, removing PVA from the formulation has proven challenging due to its perceived permanent adsorption at the interface between the organic and external aqueous phases. To prevent this, around 1.5% of PVA is used in the external aqueous phase during the process. Subsequently, the nanoparticles were subjected to a washing step to eliminate any residual PVA [24, 54].

To measure the size distribution of the prepared AMP loaded nanoparticles, DLS was used. The average particle size of AMP loaded PLA–PEG nanoparticles was found to be 142.9 nm. PDI and zeta potential of the encapsulated peptides were determined by the Beckman particle analyzer (NANO-ZS). To confirm the shape and to image the encapsulated peptides, FE-SEM analysis was performed. As depicted in Fig. 3, the nanoparticles exhibited spherical morphology, and their average diameter was 130–180 nm, with a PDI of 0.253 and a zeta potential of – 0.90 mV. The negative zeta potential can be due to the negatively charged, long PLA blocks present on the surface of the copolymer [55]. Table 1 shows the nanoparticles encapsulation efficiency (%), with more than 95% encapsulation efficiency observed for all the formulations. The increased concentration of PVA in the external aqueous phase accounts for this heightened encapsulation efficiency. The following is an explanation for this phenomenon: a higher concentration of PVA resulted in a denser external aqueous phase, which slowed down the rate at which the peptide diffused from the internal to the external aqueous phase, impeding the mass transfer of the peptide to its surroundings. As a result, the peptide can be dispersed more equally inside the microspheres, increasing the ability of the peptide to be encapsulated [56].

Translational challenges associated with nanoparticles include scalability issues and regulatory considerations. Large scale production of nanoparticles is carried out via high pressure homogenization and microfluidics. These methods ensure uniform particle sizes (~ 100–200 nm) and reproducibility across large batches, essential for maintaining consistency which is critical for therapeutic efficacy. Characterization of nanoparticles, including size distribution, zeta potential, drug loading efficiency, and surface properties, is essential for regulatory compliance and ensuring nanoparticle quality and consistency. Further, in vivo biodistribution and pharmacokinetics are also necessary to establish safety profiles. The production of nanoparticles for large scale requires compliance to Good Manufacturing Practice (GMP) standards. Stability, sterility and adherence to guidelines are other key aspects that must be addressed to ensure the nanoparticles meet regulatory requirements for clinical use. Finally, robust preclinical studies

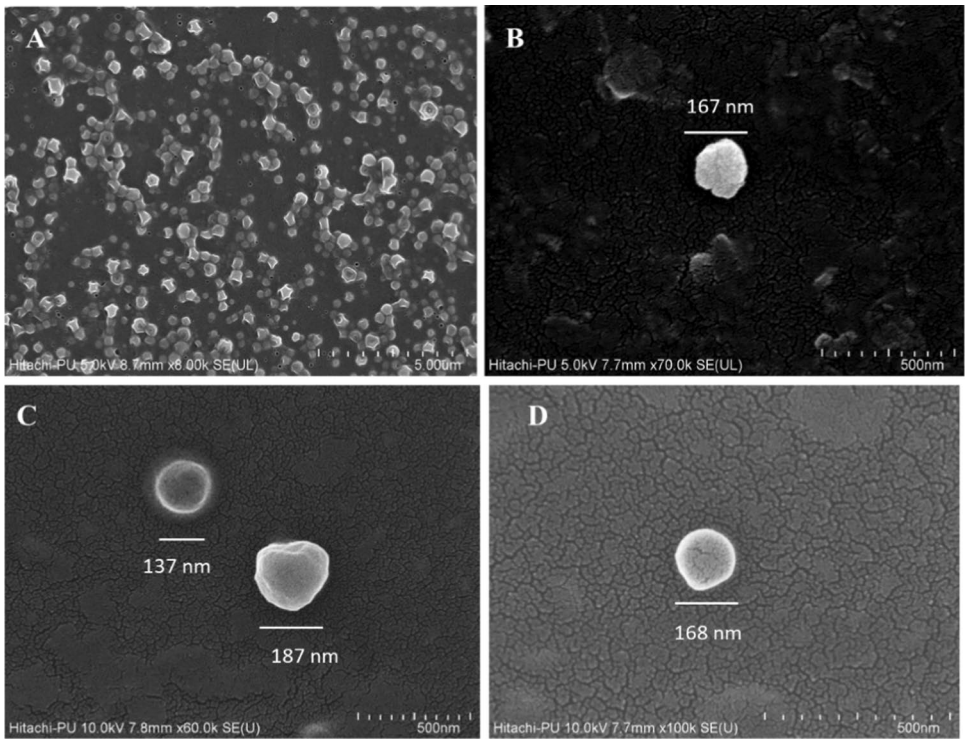

Fig. 3 **A** FE-SEM images of encapsulated peptides (**B**, **C** and **D**) coated with metal plasma and examined using Hitachi 4500 electron microscope on a carbon conductive tab, secured atop an aluminium sample disk holder (FESEM Model SU 8010 Series)

Table 1 Encapsulation efficiency of nanoparticles E-WT (S-WT NPs), E1 (analogue S1 NPs) and E2 (analogue S2 NPs)

Nanoparticles	Encapsulation efficiency (%)
E-WT NPs	96.51
E1 NPs	95.75
E2 NPs	96.48

are necessary to confirm safety and efficacy in animal models. Partnerships with industry for large-scale production are crucial to ensure the production process is scalable and cost-effective. Validation at each stage is necessary to meet regulatory standards, ultimately enabling PLA–PEG nanoparticles to become reliable therapeutic platform [57]

PLA–PEG nanoparticles are advantageous over conventional polymeric carriers like Poly (lactic-co-glycolic acid) (PLGA), chitosan, polycaprolactone (PCL), and polymethyl methacrylate (PMMA). While PLGA offers good biodegradability, it often faces challenges with burst release and acidic degradation products that can affect peptide stability. Chitosan, despite its mucoadhesive properties, shows limited control over release kinetics and exhibits lower encapsulation efficiencies compared to PLA–PEG. PEGylation in PLA–PEG provides hydrophilic/hydrophobic balance, resulting in better colloidal stability and prolonged circulation times than PCL or PMMA systems. Additionally, amphiphilic nature of PLA–PEG enables better peptide accommodation and controlled release compared to hydrophobic polymers like polyhydroxybutyrate (PHB) or polyvinyl alcohol (PVA). The surface modification potential of PLA–PEG also surpasses that of other polymeric systems, allowing for enhanced targeting capabilities and reduced immunogenicity [58]

3.3 FTIR spectra of free and encapsulated peptides

Figure 4 shows major peaks for S-WT and analogues (S1, S2) observed at 3450 cm^{-1} (Strong O–H stretching), 1642 cm^{-1} (medium C=C stretching) and 698 cm^{-1} (strong C=C bending). When these results are compared to the encapsulated peptide nanoparticles spectrum, the existence of peptide-specific peaks in the nanoparticles spectrum shows that the peptides were successfully loaded into the nanoparticles. The presence of the O–H and C=C peaks in the nanoparticle spectrum confirms that the peptides maintained their structural integrity during the encapsulation process.

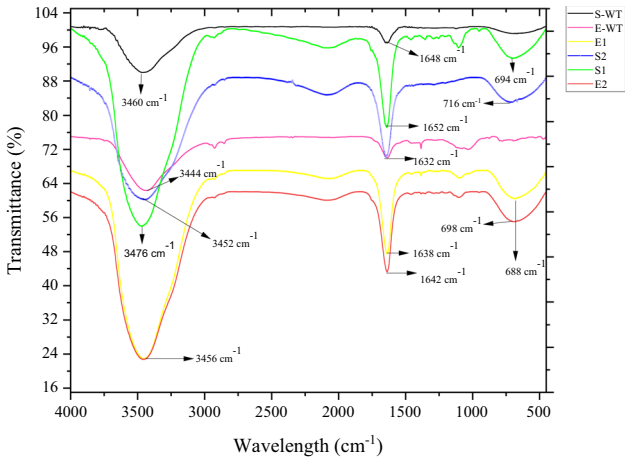

Fig. 4 FTIR spectra of free peptides (S-WT), analogues (S1 and S2)) and encapsulated peptides (Stigmurin NPs (E-WT), analogues (E1 and E2))

3.4 Molecular docking

3.4.1 Molecular docking of TasA with Stigmurin peptides

TasA protein (PDB: 5OF1) responsible for biofilm formation by *Bacillus subtilis* was docked with Stigmurin peptides (S-WT, S1 and S2) to determine the interaction of the peptide with the target protein. Docking was performed via the HADDOCK server. Among all the peptides, S2 exhibited the highest negative HADDOCK score (– 73.4 ± 3.1) and Z score (– 1.6) (given in Table 2). Further, binding affinity of S2 peptide was noted to be – 73.4, highest among the three peptides. The total energy for TasA-S2 complex was calculated to be – 223.9 kcal/mol (Table 2). This reflects good binding between the target protein and the S2 peptide. Residues of the TasA protein, such as Asp174 and Asp190, Phe191, and Asp192 are involved in interaction with Lys3 of the S2 peptide (Fig. 5). Asp174 of TasA is also involved in interactions with residues of S-WT and S1 peptides. Apart from this, Tyr124 and Lys186 of TasA interact with Phe1, Phe2, Ser3, Ile13 and Ser14 of S-WT. On the other hand, Thr189 of TasA interacts with Phe1 of S1 peptide. The active site residues are shown in blue and red colors (Fig. 5). The detailed interaction map of TasA protein with all the peptides is shown in Supplementary Fig. 3.

3.4.2 Molecular docking of Lectin LecA with Stigmurin peptides

Lectin LecA (PDB: 4LKD) is involved in biofilm formation by *Pseudomonas aeruginosa*. This protein chosen as a receptor was docked with Stigmurin peptides (S-WT, S1 and S2). S2 peptide exhibited the highest negative HADDOCK score of – 79.3 ± 0.8. The Z score value for S2 is – 1.7. Glu5, Ser111, and Ser113 are involved in hydrogen bonding interactions with Lys3 of the S2 peptide, while Gly32 interacts with Phe1, and Asn115 interacts with Pro6 of the peptide (Fig. 6). Gly32 along with Trp42 and Gly43 interact with Ser7, Ser3 and Phe2 of S-WT, while Trp33 of LecA interacts with Ile13 of S1 peptide. The active site residues are shown in blue and green colors (Fig. 5). The interaction map for Lectin LecA protein and all the peptides is shown in Supplementary Fig. 4.

Table 2 Parameters obtained after docking of Stigmurin peptide and its analogues with proteins involved in biofilm formation

S. No	Best fit cluster with target proteins		S-WT	S1	S2
1	HADDOCK score	5OF1	– 63.5 ± 10.7	– 62.1 ± 2.5	– 73.4 ± 3.1
		4LKD	– 75.3 ± 2.1	– 72.1 ± 1.5	– 79.3 ± 0.8
2	Z-Score	5OF1	– 1.3	– 0.7	– 1.6
		4LKD	– 2.2	– 1.5	– 1.7
3	Binding affinity	5OF1	– 63.5	– 63.04	– 73.4
		4LKD	– 77.67	– 73.71	– 80.12
4	Total energy	5OF1	– 162.7	– 118.7	– 223.9
		4LKD	– 98.5	– 89.7	– 167.7

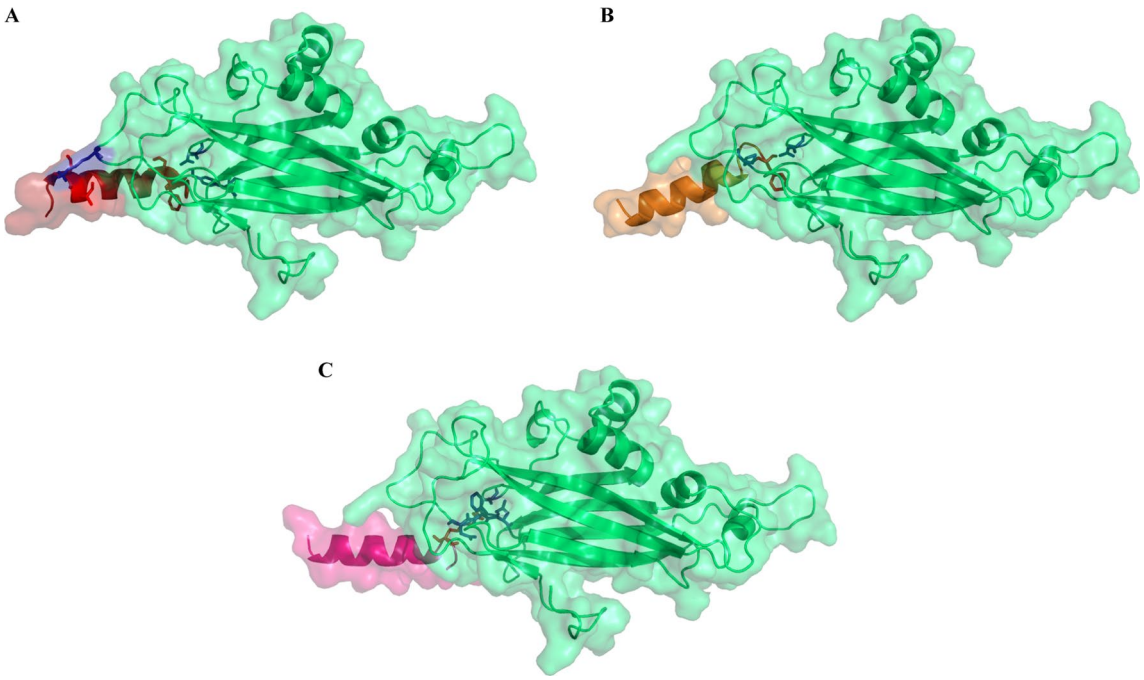

Fig. 5 Depiction of binding pose **A** TasA-S-WT **B** TasA-S1 **C** TasA-S2. Figure are generated using PyMol. The residues involved in interactions are shown in red (peptide) and blue (TasA)

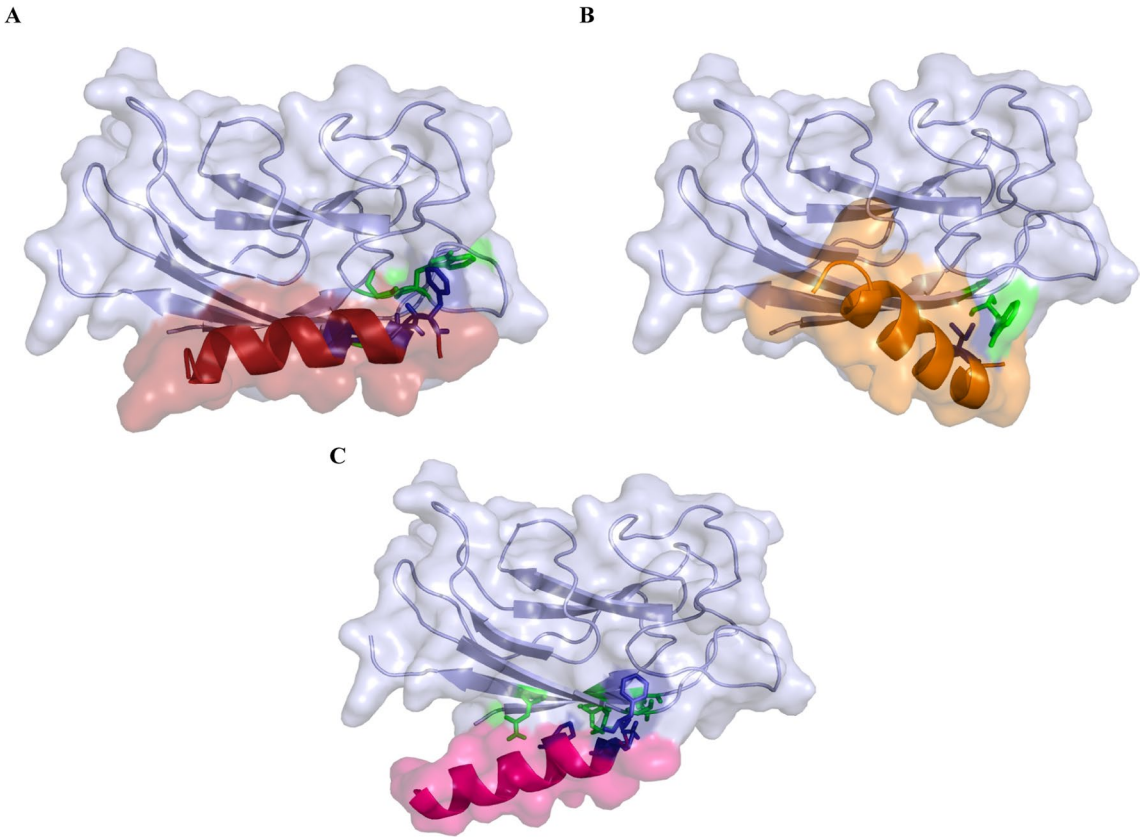

Fig. 6 Depiction of binding pose **A** Lectin LecA-S-WT (PDB: 4LKD) **B** Lectin LecA-S1 **C** Lectin LecA-S2. Figure are generated using PyMol. The residues involved in interactions are shown in blue (peptide) and green (Lectin LecA)

Various AMPs exhibit different mechanism of action against bacteria. Stigmurin exerts its effect via interaction with the bacterial membranes. Docking results revealed good binding of Stigmurin and its analogues S1 and S2 with bacterial proteins involved in biofilm formation.

3.5 Molecular dynamics simulations

3.5.1 TasA-S2 complex

MD simulations were carried out for TasA protein, S2 peptide, and the protein-peptide complex (TasA-S2 complex) depicted graphically in Fig. 7. The average RMSD for the complex was 0.45 nm, which is within the acceptable range and reveals stable binding of the peptide with the protein in the provided simulation environment. The RMSD for the free peptide increased sharply for the first few nanoseconds, followed by a drop in the value till about 10 ns. Throughout the trajectory, the peptide exhibited mild deviations, with an average value of 0.43 nm. TasA protein exhibited a slightly higher RMSD value of 0.51 nm as compared to the peptide RMSD and the RMSD for the protein-peptide complex. However, this also lies in the acceptable limit (Fig. 7A).

The radius of gyration reflects the compactness of the biomolecule. In Fig. 7B, the TasA protein exhibited an Rg value of 1.72 nm with mild fluctuations, while the peptide had an Rg value of 0.74 nm, which reflects a more rigid peptide structure. Higher Rg values are associated with decreased stability of the biomolecule. Rg value for the complex was

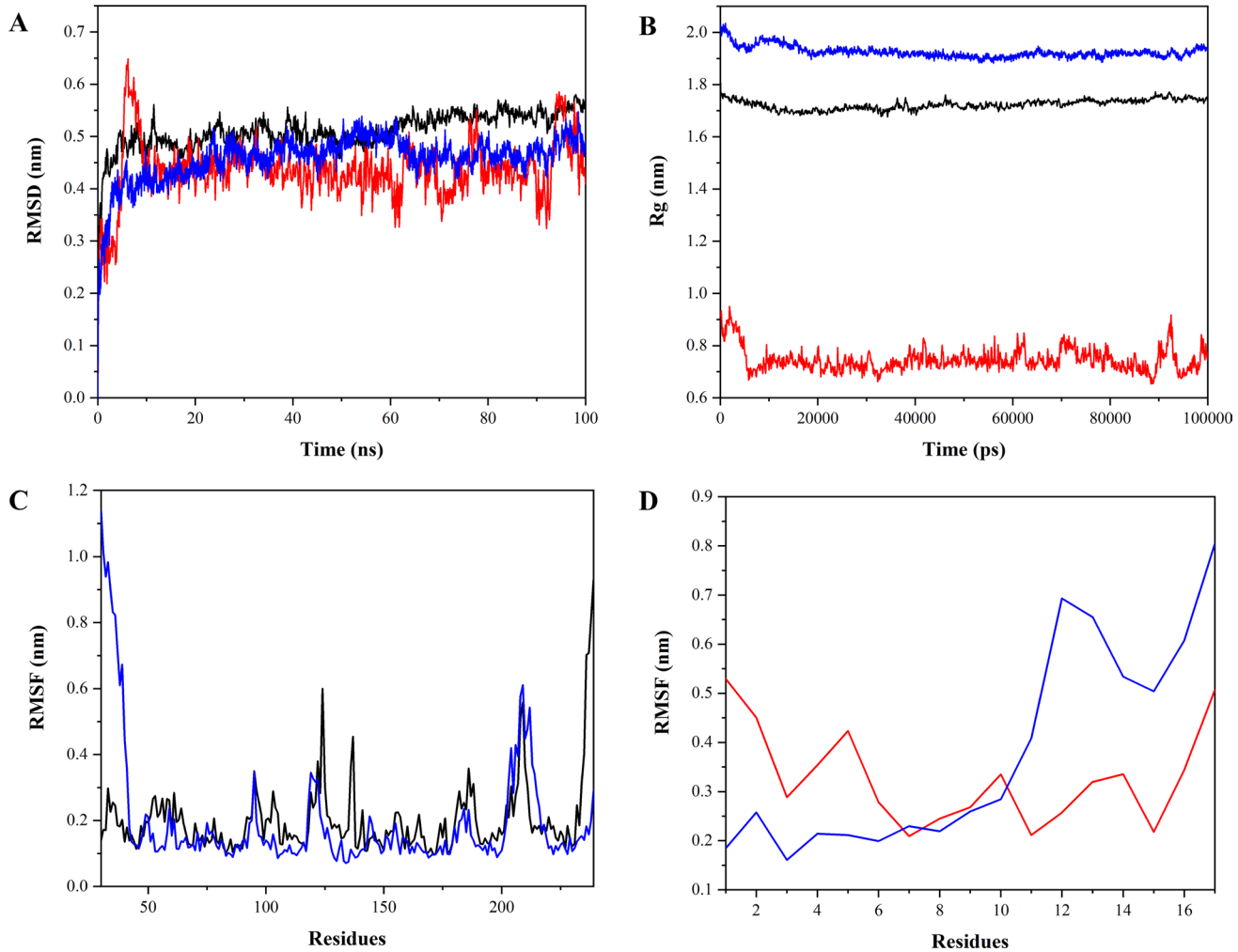

Fig. 7 Molecular Dynamics simulation performed for TasA-S2 complex for 100 ns. TasA is depicted in black, S2 in red and the TasA-S2 complex in blue. A) RMSD for TasA, peptide and TasA-S2 complex B) Rg for TasA, peptide and TasA-S2 complex C. RMSF for TasA (black) and TasA-S2 complex (blue) D. RMSF for S2 (red) and TasA-S2 complex (blue)

almost constant at 2 nm throughout the trajectory of 100 ns, indicating that the complex is stable. The overall complex exhibited a slightly higher value than the Rg for protein and peptide, which could be due to its reduced compactness.

RMSF analysis revealed that the residues were almost stable throughout the trajectory. Comparison of the data for the free protein (TasA) and the complex (TasA-S2) revealed no significant differences except for the initial few residues in the complex, which showed fluctuations. Terminal residues of the protein exhibited increased value at the end of the simulation. The average RMSF for TasA and the protein-peptide complex were 0.2 nm and 0.19 nm, respectively (Fig. 7C). These values are within the acceptable range and indicate that the complex formed is stable. However, the average RMSF for the S2 peptide and protein-peptide complex were noted to be slightly higher at 0.32 nm and 0.37 nm, respectively (Fig. 7D). Fluctuations were observed for the complex from residues 10–17. Higher RMSF values are indicative of increased flexibility during simulation. Further, SASA plots were prepared for the free TasA protein, free S2 peptide as well as TasA-S2 complex (Supplementary Fig. 5A). SASA values were also calculated for the free TasA protein, free S2 peptide as well as TasA-S2 complex before the start of the simulation as well after the 100 ns simulation. The average SASA value for free TasA protein was noted to be 100.2 nm^2, whereas for free S2 and TasA-S2 complex, the SASA values were noted to be 18.8 nm^2 and 117.68 nm^2, respectively. The complex exhibited lower SASA values than the combined average SASA values of TasA protein and S2 peptide. The SASA value for the TasA-S2 complex at the end of simulation was noted to be lower than at the start of the run, which corresponds to increased stability of the protein-peptide complex.

3.5.2 Lectin LecA-S2 complex

MD simulations were performed for the Lectin LecA protein, S2 peptide, and the protein-peptide complex (Lectin LecA-S2 complex), as shown in Fig. 8. For S2, except for the initial variations for 10 ns, RMSD was noted to be 0.43 nm for the entire simulation period. Whereas the RMSD for the protein was comparatively lower, and the average RMSD was 0.22 nm, which is within acceptable limit. Except for the minor fluctuations for the initial 40 ns, RMSD was mostly stable. The Lectin LecA-S2 complex RMSD showed fluctuations throughout the trajectory like the peptide RMSD. The complex RMSD showed a leap till 10 ns, with an average value of 0.37 nm. The RMSD values are within acceptable limits, highlighting that a stable complex forms between the protein and peptide (shown in Fig. 8A).

The Rg value for the S2 peptide was lower than the protein and the Lectin LecA -S2 complex, as shown in Fig. 8B. Rg value for S2 was almost stable at 0.74 nm and indicates its compact structure. Interestingly, both Lectin LecA and Lectin LecA-S2 complex had higher but constant Rg values of 1.43 nm and 1.49 nm, respectively, throughout the trajectory of 100 ns. This can be attributed to the compactness of the protein as well as the protein-peptide complex formed.

RMSF analysis for free protein (Lectin LecA) and protein-peptide complex (Lectin LecA-S2 complex) revealed values for the free protein and complex to be 0.13 nm and 0.11 nm, respectively. RMSF for the complex and the protein overlap except for increased RMSF of residues 100–110 of Lectin LecA. Similar RMSF values indicate the stability of the protein-peptide complex (Fig. 8C). However, for the free peptide, RMSF was 0.32 nm, while RMSF for the complex (Lectin LecA-S2 complex) was slightly higher (0.4 nm). Similar to RMSF data for S2 with the TasA-S2 complex shown above, residues from 11 to 17 have higher fluctuations, increasing the overall flexibility of the complex (Fig. 8D). Further, SASA plots were prepared for the free LecA protein, free S2 peptide as well as LecA-S2 complex (Supplementary Fig. 5B). SASA values were also calculated for the free LecA protein, free S2 peptide as well as LecA-S2 complex before the start of the simulation as well after the 100 ns simulation. The average SASA value for free LecA protein was noted to be 71.3 nm^2, while for free S2 peptide and LecA-S2 complex, the SASA values were noted to be 18.8 nm^2 and 79.16 nm^2, respectively. The SASA value for LecA-S2 complex is lower than the combined SASA value of the protein and peptide. Further, in case of the complex, it was noted that SASA value at the start and end of the simulation run remained the same, indicating stability of the LecA-S2 complex.

3.6 Antimicrobial activity

S-WT exhibited a high MIC value (> 125 µM) (Fig. 9A) against *Bacillus subtilis*, whereas the analogues S1 and S2 demonstrated significantly better antimicrobial activity with MIC values of 3.5 µM (Fig. 9B, C). This improvement highlights the effectiveness of sequence modifications in enhancing the antimicrobial properties of S1 and S2 (Supplementary Fig. 6). The increased net charge and hydrophobicity of the analogues likely enhance their interaction with bacterial membranes, promoting pore formation and subsequent cell lysis [59] Comparatively, certain scorpion AMPs, such as Pandinin 1 and 2 from *Pandinus imperator* and Imcroporin from *Isometrus maculatus*, have also shown antimicrobial activity, with MIC values of 5.2 µM, 4.8 µM, and 50 µM, respectively, against *B. subtilis* [60, 61].

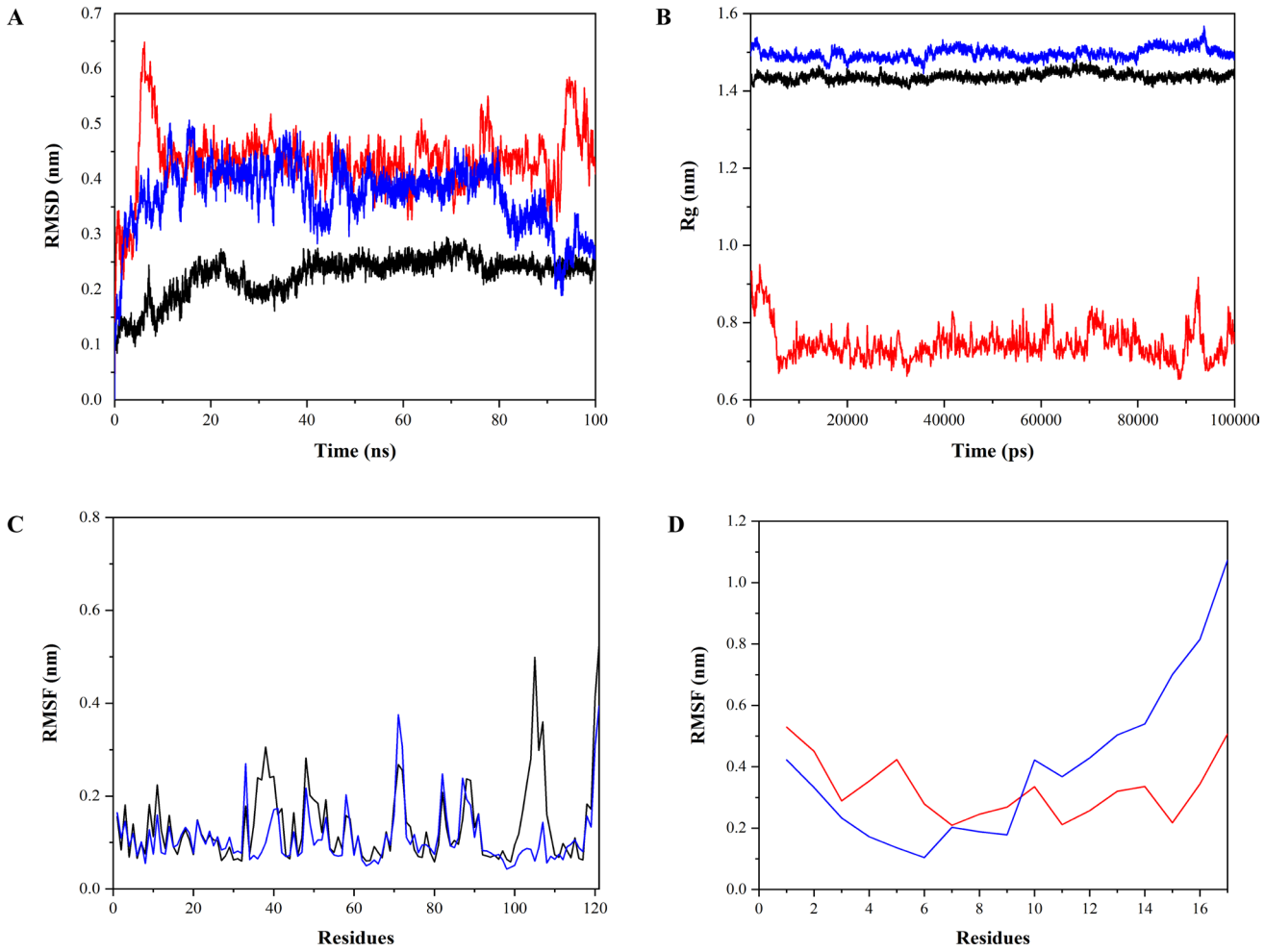

Fig. 8 Molecular Dynamics simulation performed for Lectin LecA-S2 complex for 100 ns. Lectin LecA is depicted in black, S2 in red and the Lectin LecA-S2 complex in blue. **A** RMSD for Lectin LecA, peptide and Lectin LecA-S2 complex **B** Rg for Lectin LecA, peptide and Lectin LecA-S2 complex **C** RMSF for Lectin LecA (black) and Lectin LecA-S2 complex (blue) **D** RMSF for S2 (red) and Lectin LecA -S2 complex (blue)

MBC for S-WT was not determined due to its high MIC value, but differences in bactericidal concentrations were observed for S1 and S2. S1 displayed an MBC of 21 µM, while S2 exhibited a lower MBC of 10.5 µM (Fig. 9D, E), indicating enhanced bactericidal activity in S2. In a similar study, a peptide named melittin obtained from honeybee venom showed an MBC of 30 µM against *B. subtilis* [47]. Therefore, both analogues are more effective than melittin in completely inhibiting the growth of bacteria. The difference between the MBC values of both the analogues could be due to the greater net charge and elevated hydrophobicity moment in S2, which tends to increase its interaction with the bacterial membrane, resulting in complete inhibition of bacteria at a lower concentration than S1 [10, 59] To gauge the antimicrobial effectiveness of peptides, the MBC/MIC ratio is commonly used. When the MBC/MIC ratio is ≤ 4, the outcome is characterized as bactericidal, whereas a ratio ≥ 4 is considered as bacteriostatic.[62]. Bactericidal agents typically have an MBC that closely aligns with, and generally does not exceed, four times the MIC. [63]. Earlier studies showed that Stigmurin exhibits bactericidal action on MRSA strain but shows bacteriostatic activity against the clinical strain of *S. aureus* [12]. In this study, the MBC/MIC ratio provided evidence that S1 shows bacteriostatic activity with a ratio greater than 4, and S2 shows bactericidal activity with a ratio < 4 against *B. subtilis* (Table 3).

Encapsulation of the peptides within PLA–PEG nanoparticles (E-WT, E1, E2) did not alter their MIC values (Table 3) compared to their free peptide counterparts, demonstrating that the antimicrobial activity was preserved (Supplementary Fig. 7). A similar study was done using AMP Ib – M1 and its encapsulation in polymeric nanoparticles made from alginate and chitosan, which are commonly used biocompatible polymers. The research aimed to evaluate whether the antimicrobial activity of Ib – M1 would be affected or retained upon encapsulation within these nanoparticles. It was found that the antimicrobial activity of Ib – M1 against *Escherichia coli* remained unhindered after encapsulation in the

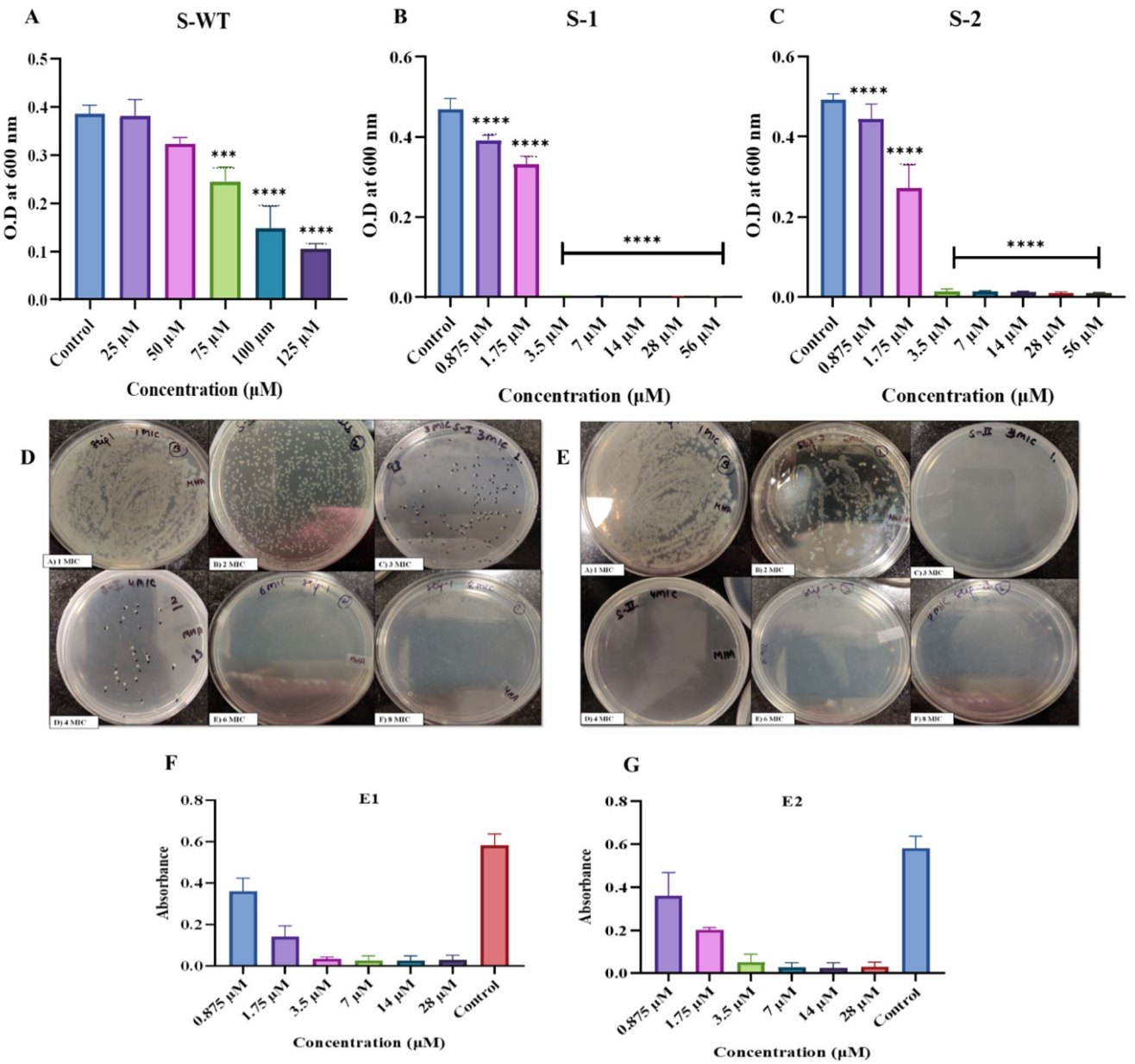

Fig. 9 MIC of the peptides against *B. subtilis* **A** > 125 µM for S-WT, **B** 3.5 µM for analogue S1, **C** 3.5 µM for analogue S2, *** $p \leq 0.001$ and **** $p < 0.0001$ compared to the positive control. Statistical analysis was performed using ANOVA followed by Tukey test. Evidence of bacterial growth was observed at all concentrations. Results shown are the average (± SD) of three independent replicates **D** Reduction in bacterial growth with increasing concentration of S1 peptide confirmed by no visible growth in the plate after 6 MIC and **E** No visible bacterial growth after 3 MIC in S2 peptide and MIC of encapsulated peptides against *B. subtilis* **F** 3.5 µM for E1 and **G** 3.5 µM for E2

Table 3 Antimicrobial activity (MIC and MBC) (MBC) of free peptide S-WT and its analogues S1 and S2 and the encapsulated peptides (E1 and E2)

Peptide	MIC (µM)	MBC
S-WT	> 125	NA
S1	3.5	21 µM
S2	3.5	10.5 µM
E1	3.5	NA
E2	3.5	NA

polymeric nanoparticles [64]. The MBC values were not determined for the encapsulated peptides because to assess the antimicrobial activity since MIC values are used as the primary metric, MBC was evaluated only for the free peptides to specifically illustrate their bactericidal concentrations. In nutshell, the encapsulated peptides (E-WT, E1, E2) exhibited the same MIC and MBC values as their free peptide counterparts, confirming that encapsulation with PLA–PEG nanoparticles did not compromise the antimicrobial efficacy of the peptides. This finding underscores the compatibility of PLA–PEG nanoparticles as a delivery system, preserving the activity of the peptides.

3.7 Hemolytic activity of Stigmurin and its analogues

S-WT, S1, and S2 were tested for their haemolytic potential in RBCs at concentrations ranging from 0.875 to 56 µM. S-WT demonstrated low hemolytic activity (2.25%) at the maximum concentration tested. In contrast, when S1 and S2 were tested at high concentrations, they induced hemolysis of around 26.4% and 29.4%, respectively (as depicted in Fig. 10A–C). The observed increase in hemolysis can be attributed to the inclusion of lysine in the sequence of the peptide. This lysine addition increases the hydrophobic moment of S1 and S2, thereby intensifying its interaction with the erythrocyte membrane [11]. Notably, at lower concentrations, where the minimum inhibitory concentration (MIC) was detected, both S1 and S2 exhibited low hemolysis, remaining below the 10% threshold.

The hemolytic activity of EWT, E1, and E2 was also determined to check the changes induced upon encapsulation of the peptides. The same concentrations were used to evaluate the hemolytic activity of the peptides. E1 (7%) and E2 (11%) showed low hemolytic activity when conjugated with PLA–PEG polymer (Fig. 10D–F) (Supplementary Fig. 8). This is especially evident when compared to Triton-X 100, employed as the positive control (PC), and PBS, utilized as the negative control (NC). A similar study provided evidence of decreased hemolytic activity after encapsulation; free D-melittin and D-melittin polymeric nanoparticles were tested against erythrocytes, and a 100-fold decrease in hemolytic activity was noted [65].

Without encapsulation, AMPs directly interact with negatively charged phospholipids, especially in erythrocytes, leading to hemolysis. Encapsulation of stigmurin and its analogues in PLA–PEG may have reduced the hemolytic activity of the peptides by preventing their interactions with erythrocyte membranes. This reduction can be achieved through the masking of the positively charged amino acids such as lysine, which otherwise can promote strong interactions with erythrocyte membrane made up of negatively charged phospholipids. Moreover, the encapsulation can provide steric

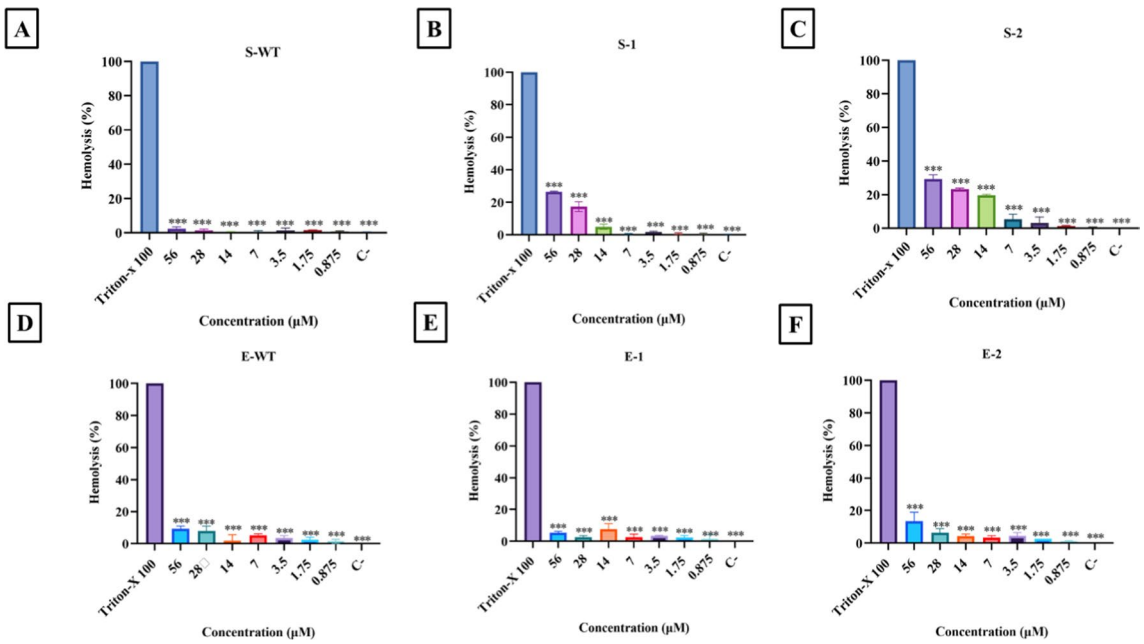

Fig. 10 Hemolytic activity of free peptides treated with B+ve human erythrocytes where C- denotes negative control containing only 1×PBS: **A** shows the low activity of S-WT peptide against erythrocytes, **B** and **C** represent the high degree of hemolysis by analogues S1 and S2 with increasing concentration. **D**, **E** and **F** reduced activity of encapsulated peptides E-WT, E1 and E2 against RBCs. To interpret the bioassays, comparisons across multiple groups using analysis of variance (ANOVA) with Graph Pad Prism software (Version 5.00, Graph Pad, San Diego, CA, USA) was done. Significance was established when the *p*-value was less than 0.0001

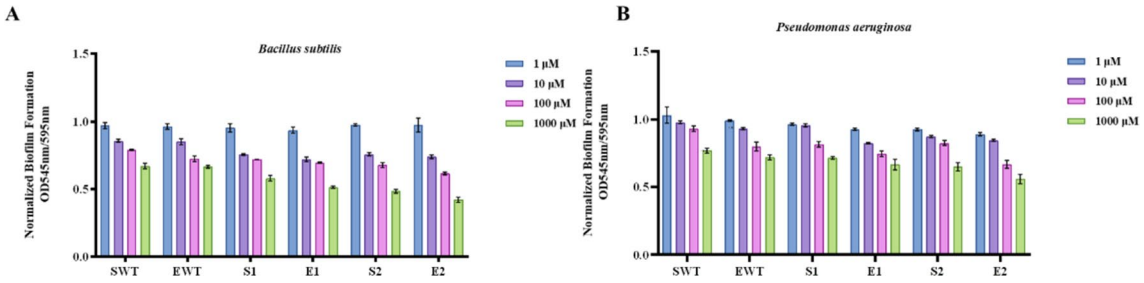

Fig. 11 Static biofilm assay exhibiting inhibitory activity of Stigmurin variants against **A** Bacillus subtilis biofilm **B** Pseudomonas aeruginosa biofilm. Biofilm formation was noted at all concentrations. Results shown are the average (± SD) of three independent replicates. Significance was established when the *p*-value was less than 0.0001. Statistical analysis was performed using 2way ANOVA followed by Tukey test

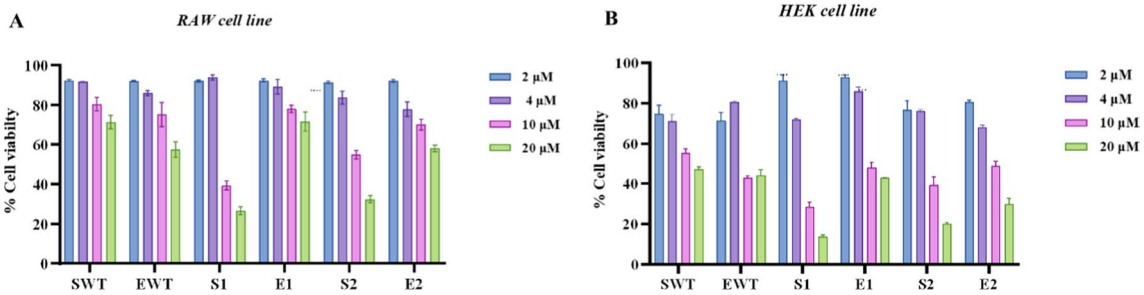

Fig. 12 **A** MTT reduction assay for the encapsulated peptides (EWT, E1, E2) and free peptides (SWT, S1, S2) in RAW 264.7 cells and **B** HEK293 cells. Results shown are the average (± SD) of three independent replicates. Significance was established when the *p*-value was less than 0.0001. Statistical analysis was performed using 2way ANOVA followed by Tukey test

hindrance, thereby blocking the physical contact directly between the peptides and cell membrane. A study showed that PEGylation of AMPs lowered cytotoxicity and hemolysis by hiding their cationic charges and limiting interactions with mammalian cells [66, 67].

3.8 Static biofilm assay

A static biofilm assay was performed for S-WT, S1, and S2, as well as the encapsulated peptides E-WT, E1, and E2, to evaluate the effectiveness of the peptides in inhibiting biofilm formation. The inhibitory potential of the peptides was tested against biofilm formation by *Bacillus subtilis* and *Pseudomonas aeruginosa; the* results are depicted in Fig. 11A, B. In the case of *B. subtilis*, among all the peptides tested for anti-biofilm activity, E2 exhibits the most promising result with maximum anti-biofilm activity at 1000 µM concentration, followed by S2 peptide. Similarly, for *P. aeruginosa* biofilm, E2 shows maximum anti-biofilm activity in comparison with other peptides. The results suggest the promising anti-biofilm potential of encapsulated S2 peptide compared to encapsulated S1 peptide and other free peptides.

Studies have demonstrated that encapsulation can significantly improve the inhibition of biofilm formation by the peptide [68] For example, thiolated chitosan nanoparticles encapsulating nisin and selenium showed enhanced antibacterial and anti-biofilm activity against multiple pathogens, including *Staphylococcus aureus* and *Escherichia coli*. This enhanced effect is attributed to the sustained release and improved stability of the encapsulated peptide [69]. Studies on nanoliposome-encapsulated antibiotics, such as Imipenem/Cilastatin, have demonstrated improved efficacy against biofilm-forming bacteria like *Pseudomonas aeruginosa*. This improvement is attributed to the controlled release of the drug and increased penetration into the biofilm matrix, leading to better biofilm eradication compared to free forms of the antibiotics [70]

3.9 Cytotoxicity activity of the peptides

The cytotoxicity of S-WT, S1, S2, E-WT, E1, and E2 was examined on RAW 264.7 cells and HEK 293 cells using MTT cell viability assay. Figure 12 shows the percent cell viability of the RAW 264.7 (A) and HEK293 cells (B) after treatment with S-WT, S1, S2, EWT, E1, and E2 as a function of concentration. S-WT, S1, and S2 had a visible toxic effect on HEK293 and

RAW 264.7 cells at 4 µM, 10 µM and 20 µM concentrations, whereas E-WT, E1, and E2 demonstrated no toxic effect on HEK293 and RAW 264.7 cells at 2 µM, 4 µM and 10 µM concentrations where 10–20% increase in cell viability was observed at these concentrations. However, a slight decrease in viability was observed at 20 µM. Further, it is evident from the above results that the free-form peptides such as S-WT, S1, and S2 exhibited considerable toxic effects on both cell lines at all the concentrations tested. In comparison, peptides encapsulated with PLA–PEG copolymers are less toxic than free peptides [71]. Conversely, at lower concentrations, slight increase in cytotoxicity was observed associated with polymer encapsulation. Notably, while the encapsulated peptides demonstrated a notable reduction in toxicity at high concentrations, increased toxicity at lower concentrations raises important considerations for therapeutic applications.

The addition of lysine to analogues raised the net charge of the peptides, enhancing their antimicrobial activity as well as their direct interaction with negatively charged components of mammalian cell membranes. Encapsulation masks these charges, limiting non-specific interactions with cell membranes. For instance, encapsulating ultrashort AMPs like arginine rich basic repeat-based residue (RBRBR) in chitosan nanoparticles significantly reduced cytotoxicity in mammalian Vero cell lines (ATCC CCL81), likely due to charge shielding [72]. PEG can provide a hydrophilic barrier that can prevent the direct contact between the peptide and the cell membrane, reducing membrane disruption and cytotoxicity [73]. Furthermore, encapsulation allows for controlled and sustained release of AMPs, ensuring therapeutic levels that are effective against pathogens while minimizing exposure to mammalian cells [74] This controlled release system was demonstrated with ciprofloxacin-loaded PEG-PLGA nanoparticles, which exhibited prolonged activity with reduced cytotoxicity [75]. Ciprofloxacin-loaded PEG-PLGA nanoparticles were used to demonstrate this controlled release technique and they showed sustained action with little cytotoxicity [73]. Without encapsulation, AMPs can interact with both bacterial and mammalian membranes indiscrimantely, increasing cytotoxicity and limiting therapeutic uses.

4 Conclusion

This study highlights the potential of AMPs as a promising alternative to antibiotics for targeting drug-resistant organisms. AMPs serve as a natural line of defense in many organisms and hold great therapeutic potential. However, their application is often limited by challenges such as increased hemolytic activity and rapid degradation, particularly in analogues designed to enhance antimicrobial efficacy. Addressing this limitation is crucial for the safe and effective use of AMPs in clinical settings.

In our study, Stigmurin and its analogues were successfully synthesized using Fmoc solid-phase peptide chemistry. To overcome their limitations, the PLA–PEG di-block copolymer was synthesized for peptide encapsulation. PLA–PEG copolymer, with its amphiphilic nature, maintained the physical and chemical properties of the peptides, as confirmed by characterization studies using NMR and FTIR. Peptide loaded nanoparticles were prepared using the double emulsion solvent evaporation method, achieving a uniform size range of 160–180 nm and efficient peptide encapsulation, as validated by FESEM and encapsulation efficiency analysis. Importantly, the antimicrobial activity of the peptides remained unaffected by encapsulation, as demonstrated by comparable activity between free peptides and their encapsulated counterparts. Furthermore, the encapsulated E2 peptide exhibited better antibiofilm activity compared to its free counterpart (S2), effectively inhibiting biofilm formation by *Bacillus subtilis* and *Pseudomonas aeruginosa*. Increased hemolysis (30%) was observed in the analogues (S1 and S2), which is due to the incorporation of hydrophobic amino acids in the peptide backbone to increase antimicrobial activity. In contrast, the encapsulated peptides showed reduced hemolysis which addresses the main concern of the study for their safer therapeutic use. Additionally, encapsulated peptides exhibited reduced cytotoxicity toward RAW 264.7 and HEK293 cells compared to free peptides, further validating the potential of PLA–PEG as safer delivery systems.

The mechanism of action of Stigmurin and its analogues, characterized by membrane disruption through interactions with negatively charged bacterial membranes, aligns closely with our in silico findings. Molecular docking analysis revealed strong interactions between Stigmurin peptides and target proteins TasA and Lectin LecA, which are crucial for biofilm formation. This supports the hypothesis that the cationic and amphipathic nature of Stigmurin facilitates effective binding to bacterial targets. Moreover, the enhanced positive charge and hydrophobicity in the analogues S1 and S2 not only improved their antimicrobial activity, as observed experimentally, but also contributed to stronger interactions with biofilm-associated proteins as noted via in silico studies. These findings suggest that the physicochemical properties responsible for membrane disruption also enhance biofilm inhibition by targeting critical bacterial proteins.

Despite the promising findings of this study, there are some limitations, and addressing these can pave way for clinical translation. The study involved in silico approach of binding of Stigmurin and its analogues with bacterial proteins (*B.*

subtilis and *P. aeruginosa*) involved in biofilm formation. The study focused on *B. subtilis* and *P. aeruginosa*, highlighting the need to evaluate the activity of the peptides against a broader range of clinically relevant pathogens. Additionally, the stability of the nanoparticles in complex biological environments and the scalability of the encapsulation process for large-scale production require further experimentation. Furthermore, while cytotoxicity was reduced in vitro, the long-term toxicity, biocompatibility and fate of the nanoparticles in vivo remain unexplored. Future research could explore the pharmacokinetics, biodistribution and efficacy of these encapsulated peptides in animal models to further validate their potential. Addressing these limitations in future studies will be essential for advancing this approach toward clinical applications.

This study provides a strong foundation for translating these findings in vivo for broader therapeutic applications. PLA–PEG encapsulation strategy offers a pathway for advancing AMPs as viable treatments against drug-resistant pathogens and associated infections, while mitigating safety concerns.

Acknowledgements GS and RPB acknowledge the financial supports from UGC-Faculty recharge program and ICMR-DHR International Fellowship for Senior Scientists (2023-24), DBT (BT/PR27444/BRB/10/1645/2018), DST (DST/CSRI/2021/7), DST-SERB (CRG/2022/000628), ICMR (17X(3)/Ad-hoc/69/2022-ITR), CSIR (37/1743/23/EMR-II), DHR start up (R.12020/02/2024-HR/E-Office:8292859), and ICMR (35/2/2020-Nano/BMS), Government of India. HKA and AS acknowledge DHR, Government of India (YSS/2020/000047/PRCYSS) and ICMR, Government of India (HIV/STI/18/02/2022-ECD-II), respectively for the financial support. The cell culture facility at UIPS, Panjab University is duly acknowledged.

Author contributions AT: Data curation, Formal analysis, Methodology, Investigation, Software, Validation, Visualization, Writing-original draft. HKA: Data curation, Formal analysis, Investigation, Validation, Writing-original draft. AS: Data curation, Formal analysis, Methodology, Investigation, Software, Validation, Visualization, Writing-review and editing. EH: Data curation, Formal analysis, Methodology, Investigation. AK: Data curation, Methodology. LK: Data curation, Methodology. PKJ: Data curation, Formal analysis, Methodology, Investigation, Writing-original draft. YbL: Conceptualization, Methodology, Software, Funding acquisition, Writing-review and editing. GS: Conceptualization, Methodology, Investigation, Writing-review and editing, Supervision, Project administration, Funding acquisition. RPB: Conceptualization, Methodology, Software, Resources, Investigation, Writing-review and editing, Supervision, Project administration, Funding acquisition, Visualization. All authors read and approved the manuscript for publication.

Funding UGC, New Delhi, India, under Faculty Recharge Program, ICMR-DHR International Fellowship for Senior Scientists (2023-24), DBT (BT/PR27444/BRB/10/1645/2018), DST (DST/CSRI/2021/7), DST-SERB (CRG/2022/000628), ICMR (17X(3)/Ad-hoc/69/2022-ITR), CSIR (37/1743/23/EMR-II), DHR start up (R.12020/02/2024-HR/E-Office:8292859)), and ICMR (35/2/2020-Nano/BMS), DHR (YSS/2020/000047/PRCYSS) and ICMR (HIV/STI/18/02/2022-ECD-II).

Data availability The data in current study are available from the corresponding author on request.

Code availability None.

Declarations

Ethical approval and consent to participate The work was approved by PGIMER Institutional Ethics Committee (Ethical Clearance Number: PGI/IEC/2022/000734). Consent from the donors were obtained. All experiments were performed in accordance with relevant guidelines and regulations. Informed consent for study participation were obtained from the donors.

Consent for publication All authors read and approved the final manuscript.

Competing interests RPB is Editorial Board Members for this journal.

References

1. Fontanot A, Ellinger I, Unger WWJ, Hays JP. A comprehensive review of recent research into the effects of antimicrobial peptides on biofilms—January 2020 to September 2023. Antibiotics. 2024. https://doi.org/10.3390/antibiotics13040343.
2. Hancock REW. Peptide antibiotics. Lancet. 1997;349:418–22. https://doi.org/10.1016/S0140-6736(97)80051-7.

3. Thakur A, Sharma A, Alajangi HK, Kumar P, Lim Y, Singh G, Pratap R. International Journal of Biological Macromolecules In pursuit of next-generation therapeutics : antimicrobial peptides against superbugs, their sources, mechanism of action, nanotechnology-based delivery, and clinical applications. Int J Biol Macromol. 2022;218:135–56. https://doi.org/10.1016/j.ijbiomac.2022.07.103.
4. Zasloff M. Antimicrobial peptides of multicellular organisms. Nature. 2002;415:389–95. https://doi.org/10.1038/415389a.
5. Rozek A, Friedrich RE. Structure of the bovine antimicrobial peptide indolicidin bound to dodecylphosphocholine and sodium dodecyl sulfate micelles. Biochemistry. 2000;39:15765–74.
6. Tonk M, Vilcinskas A, Rahnamaeian M. Insect antimicrobial peptides: potential tools for the prevention of skin cancer. Appl Microbiol Biotechnol. 2016;100:7397–405. https://doi.org/10.1007/s00253-016-7718-y.
7. Min KH, Kim KH, Ki M-R, Pack SP. Antimicrobial peptides and their biomedical applications: a review. Antibiotics. 2024;13:794. https://doi.org/10.3390/antibiotics13090794.
8. Raghuraman H, Chattopadhyay A. Melittin: a membrane-active peptide with diverse functions. Biosci Rep. 2007;27:189–223. https://doi.org/10.1007/s10540-006-9030-z.
9. Lopes D, Geovana P, Leite Q, Rodrigo A, Da R. Thermal characterization of antimicrobial peptide stigmurin employing thermal analytical techniques. J Therm Anal Calorim. 2019;138:3765–79.
10. De Melo ET, Estrela AB, Santos ECG, Machado PRL, Farias KJS, Torres TM, Carvalho E, Lima JPMS, Silva-Júnior AA, Barbosa EG, Fernandes-Pedrosa MDF. Structural characterization of a novel peptide with antimicrobial activity from the venom gland of the scorpion Tityus stigmurus: Stigmurin. Peptides. 2015;68:3–10. https://doi.org/10.1016/j.peptides.2015.03.003.
11. Parente AMS, Daniele-silva A, Furtado AA, Melo MA, Lacerda AF, Queiroz M, Santos E, Rocha HAO, Barbosa G, Carvalho E, Silva-j AA, Silva MS, Fernandes-pedrosa MDF. Analogs of the scorpion venom peptide stigmurin : structural assessment, toxicity, and increased. Toxins. 2018. https://doi.org/10.3390/toxins10040161.
12. Daniele-Silva A, Machado RJA, Monteiro NKV, Estrela AB, Santos ECG, Carvalho E, Araújo Júnior RF, Melo-Silveira RF, Rocha HAO, Silva-Júnior AA, Fernandes-Pedrosa MF. Stigmurin and TsAP-2 from Tityus stigmurus scorpion venom: assessment of structure and therapeutic potential in experimental sepsis. Toxicon. 2016;121:10–21. https://doi.org/10.1016/j.toxicon.2016.08.016.
13. Amorim-Carmo B, Daniele-Silva A, Parente AMS, Furtado AA, Carvalho E, Oliveira JWF, Santos ECG, Silva MS, Silva SRB, Silva-Júnior AA, Monteiro NK, Fernandes-Pedrosa MF. Potent and broad-spectrum antimicrobial activity of analogs from the scorpion peptide stigmurin. Int J Mol Sci. 2019;20:1–21. https://doi.org/10.3390/ijms20030623.
14. Daniele-Silva A, de Rodrigues SCS, dos Santos ECG, de QueirozNeto MF, de Rocha HAO, da Silva-Júnior AA, Resende JM, Araújo RM, de Fernandes-Pedrosa MF. NMR three-dimensional structure of the cationic peptide Stigmurin from Tityus stigmurus scorpion venom: In vitro antioxidant and in vivo antibacterial and healing activity. Peptides. 2021. https://doi.org/10.1016/j.peptides.2020.170478.
15. Drayton M, Kizhakkedath JN, Strau SK. Towards robust delivery of antimicrobial peptides to combat bacterial resistance. Molecules. 2020. https://doi.org/10.3390/molecules25133048.
16. Qi W, Li T, Zhang Z, Wu T. Preparation and characterization of oleogel-in-water pickering emulsions stabilized by cellulose nanocrystals. Food Hydrocoll. 2021;110: 106206. https://doi.org/10.1016/J.FOODHYD.2020.106206.
17. Lee IM, Li WC, Chu YC. Amphiphilic poly(D, L-lactic acid)/poly(ethylene glycol)/poly(D, L-lactic acid) nanogels for controlled release of hydrophobic drugs. Macromol Biosci. 2006;6:846–54. https://doi.org/10.1002/mabi.200600101.
18. Mundel R, Thakur T, Chatterjee M. Emerging uses of PLA–PEG copolymer in cancer drug delivery. 3 Biotech. 2022. https://doi.org/10.1007/s13205-021-03105-y.
19. Vlachopoulos A, Karlioti G, Balla E, Daniilidis V, Kalamas T, Stefanidou M, Bikiaris ND, Christodoulou E, Koumentakou I, Karavas E, Bikiaris DN. Poly(lactic acid)-based microparticles for drug delivery applications: an overview of recent advances. Pharmaceutics. 2022. https://doi.org/10.3390/pharmaceutics14020359.
20. Peng C, Wang Q, Xu W, Wang X, Zheng Q, Liang X, Dong X, Li F, Peng L. A bifunctional endolytic alginate lyase with two different lyase catalytic domains from Vibrio sp. H204. Front Microbiol. 2024. https://doi.org/10.3389/fmicb.2024.1509599.
21. Ghasemiyeh P, Mohammadi-Samani S. Polymers blending as release modulating tool in drug delivery. Front Mater. 2021. https://doi.org/10.3389/fmats.2021.752813.
22. Garofalo C, Capuano G, Sottile R, Tallerico R, Adami R, Reverchon E, Carbone E, Izzo L, Pappalardo D. Different insight into amphiphilic PEG-PLA copolymers: influence of macromolecular architecture on the micelle formation and cellular uptake. Biomacromol. 2014;15:403–15. https://doi.org/10.1021/bm401812r.
23. Kumar M, Gupta D, Singh G, Sharma S, Bhat M, Prashant CK, Dinda AK, Kharbanda S, Kufe D, Singh H. Novel polymeric nanoparticles for intracellular delivery of peptide cargos: antitumor efficacy of the BCL-2 conversion peptide NuBCP-9. Cancer Res. 2014;74:3271–81. https://doi.org/10.1158/0008-5472.CAN-13-2015.
24. Jain AK, Goyal AK, Gupta PN, Khatri K, Mishra N, Mehta A, Mangal S, Vyas SP. Synthesis, characterization and evaluation of novel triblock copolymer based nanoparticles for vaccine delivery against hepatitis B. J Control Release. 2009;136:161–9. https://doi.org/10.1016/j.jconrel.2009.02.010.
25. Piras AM, Maisetta G, Sandreschi S, Gazzarri M, Bartoli C, Grassi L, Esin S, Chiellini F, Batoni G. Chitosan nanoparticles loaded with the antimicrobial peptide temporin B exert a long-term antibacterial activity in vitro against clinical isolates of Staphylococcus epidermidis. Front Microbiol. 2015;6: 135235. https://doi.org/10.3389/FMICB.2015.00372/BIBTEX.
26. Tanaka K, Kuramochi H, Maeda K, Takahashi Y, Osako M, Suzuki G. Size-controlled preparation of polyethylene nanoplastic particles by nanoprecipitation and insights into the underlying mechanisms. ACS Omega. 2023;8:14470–7. https://doi.org/10.1021/acsomega.2c08233.
27. Mahmood S, Mandal UK, Chatterjee B, Taher M. Advanced characterizations of nanoparticles for drug delivery: Investigating their properties through the techniques used in their evaluations. Nanotechnol Rev. 2017;6:355–72. https://doi.org/10.1515/NTREV-2016-0050/ASSET/GRAPHIC/J_NTREV-2016-0050_FIG_007.JPG.
28. Danaei M, Dehghankhold M, Ataei S, Hasanzadeh Davarani F, Javanmard R, Dokhani A, Khorasani S, Mozafari MR. Impact of particle size and polydispersity index on the clinical applications of lipidic nanocarrier systems. Pharmaceutics. 2018;10:1–17. https://doi.org/10.3390/pharmaceutics10020057.

29. Emami S, Valizadeh H, Islambulchilar Z, Zakeri-Milani P. Development and physicochemical characterization of sirolimus solid dispersions prepared by solvent evaporation method. Adv Pharm Bull. 2014;4:369–74. https://doi.org/10.5681/apb.2014.054.
30. Dora CP, Singh SK, Kumar S, Datusalia AK, Deep A. Development and characterization of nanoparticles of glibenclamide by solvent displacement method. Acta Poloniae Pharmaceutica Drug Res. 2010;67:283–90.
31. Mirdita M, Schütze K, Moriwaki Y, Heo L, Ovchinnikov S, Steinegger M. ColabFold: making protein folding accessible to all. Nat Methods. 2022;19:679–82. https://doi.org/10.1038/s41592-022-01488-1.
32. Jumper J, Evans R, Pritzel A, Green T, Figurnov M, Ronneberger O, Tunyasuvunakool K, Bates R, Žídek A, Potapenko A, Bridgland A, Meyer C, Kohl SAA, Ballard AJ, Cowie A, Romera-Paredes B, Nikolov S, Jain R, Adler J, Back T, Petersen S, Reiman D, Clancy E, Zielinski M, Steinegger M, Pacholska M, Berghammer T, Bodenstein S, Silver D, Vinyals O, Senior AW, Kavukcuoglu K, Kohli P, Hassabis D. Highly accurate protein structure prediction with AlphaFold. Nature. 2021;596:583–9. https://doi.org/10.1038/s41586-021-03819-2.
33. Steinegger J, Söding M. MMseqs2 enables sensitive protein sequence searching for the analysis of massive data sets. Nat Biotechnol. 2017;35:1026–8.
34. Case DA, Cheatham TE, Darden T, Gohlke H, Luo R, Merz KM, Onufriev A, Simmerling C, Wang B, Woods RJ. The Amber biomolecular simulation programs. J Comput Chem. 2005;26:1668–88. https://doi.org/10.1002/jcc.20290.
35. Pettersen TE, Goddard EF, Huang TD, Couch CC, Greenblatt GS, Meng DM, Ferrin EC. UCSF chimera: a visualization system for exploratory research and analysis. J Comput Chem. 2004;25:1605–12.
36. Honorato AMJJ, Koukos RV, Jiménez-García PI, Tsaregorodtsev B, Verlato A, Giachetti M, Rosato A, Bonvin A. Structural biology in the clouds: the WeNMR-EOSC ecosystem. Front Mol Biosci. 2021;8:729513.
37. Laskowski RA, Swindells MB. LigPlot+: multiple ligand-protein interaction diagrams for drug discovery. J Chem Inf Model. 2011;51:2778–86. https://doi.org/10.1021/ci200227u.
38. Taghizadeh MS, Taherishirazi M, Niazi A, Afsharifar A, Moghadam A. Structure-guided design and cloning of peptide inhibitors targeting CDK9/cyclin T1 protein-protein interaction. Front Pharmacol. 2024;15:1327820. https://doi.org/10.3389/FPHAR.2024.1327820/BIBTEX.
39. Varadi M, Anyango S, Deshpande M, Nair S, Natassia C, Yordanova G, Yuan D, Stroe O, Wood G, Laydon A, Zídek A, Green T, Tunyasuvunakool K, Petersen S, Jumper J, Clancy E, Green R, Vora A, Lutfi M, Figurnov M, Cowie A, Hobbs N, Kohli P, Kleywegt G, Birney E, Hassabis D, Velankar S. AlphaFold Protein Structure Database: massively expanding the structural coverage of protein-sequence space with high-accuracy models. Nucleic Acids Res. 2022;50:D439–44. https://doi.org/10.1093/nar/gkab1061.
40. Diehl A, Roske Y, Ball L, Chowdhury A, Hiller M, Molière N, Kramer R, Stöppler D, Worth CL, Schlegel B, Leidert M, Cremer N, Erdmann N, Lopez D, Stephanowitz H, Krause E, van Rossum BJ, Schmieder P, Heinemann U, Turgay K, Akbey Ü, Oschkinat H. Structural changes of TasA in biofilm formation of Bacillus subtilis. Proc Natl Acad Sci U S A. 2018;115:3237–42. https://doi.org/10.1073/pnas.1718102115.
41. Kadam RU, Bergmann M, Garg D, Gabrieli G, Stocker A, Darbre T, Reymond JL. Structure-based optimization of the terminal tripeptide in glycopeptide dendrimer inhibitors of pseudomonas aeruginosa biofilms targeting LecA. Chem Eur J. 2013;19:17054–63. https://doi.org/10.1002/chem.201302587.
42. Van Der Spoel D, Lindahl E, Hess B, Groenhof G, Mark AE, Berendsen HJC. GROMACS: fast, flexible, and free. J Comput Chem. 2005;26:1701–18. https://doi.org/10.1002/jcc.20291.
43. Rababi D, Nag A. A top-down approach for studying the in-silico effect of the novel phytocompound tribulusamide B on the inhibition of Nipah virus transmission through targeting fusion glycoprotein and matrix protein. Comput Biol Chem. 2024;112: 108135. https://doi.org/10.1016/J.COMPBIOLCHEM.2024.108135.
44. Abohassan M, Alshahrani M, Alshahrani MY, Rajagopalan P. Insilco and Invitro approaches identify novel dual PI3K/AKT pathway inhibitors to control acute myeloid leukemia cell proliferations. Med Oncol. 2022;39:1–10. https://doi.org/10.1007/S12032-022-01846-1/METRICS.
45. Borjian Boroujeni M, Shahbazi Dastjerdeh M, Shokrgozar MA, Rahimi H, Omidinia E. Computational driven molecular dynamics simulation of keratinocyte growth factor behavior at different pH conditions. Inform Med Unlocked. 2021. https://doi.org/10.1016/j.imu.2021.100514.
46. Wiegand I, Hilpert K, Hancock REW. Agar and broth dilution methods to determine the minimal inhibitory concentration (MIC) of antimicrobial substances. Nat Protoc. 2015. https://doi.org/10.1038/nprot.2007.521.
47. Al-Ani I, Zimmermann S, Reichling J, Wink M. Pharmacological synergism of bee venom and melittin with antibiotics and plant secondary metabolites against multi-drug resistant microbial pathogens. Phytomedicine. 2015;22:245–55. https://doi.org/10.1016/j.phymed.2014.11.019.
48. De Menezes YAS, Félix-Silva J, Da Silva-Júnior AA, Rebecchi IMM, De Oliveira AS, Uchoa AF, De Fernandes-Pedrosa MF. Protein-rich fraction of cnidoscolus urens (L.) arthur leaves: Enzymatic characterization and procoagulant and fibrinogenolytic activities. Molecules. 2014;19:3552–69. https://doi.org/10.3390/molecules19033552.
49. Park S, Kim HS, Ok K, Kim Y, Park HD, Byun Y. Design, synthesis and biological evaluation of 4-(alkyloxy)-6-methyl-2H-pyran-2-one derivatives as quorum sensing inhibitors. Bioorg Med Chem Lett. 2015;25:2913–7. https://doi.org/10.1016/j.bmcl.2015.05.054.
50. Zerin T, Kim JS, Gil HW, Song HY, Hong SY. Effects of formaldehyde on mitochondrial dysfunction and apoptosis in SK-N-SH neuroblastoma cells. Cell Biol Toxicol. 2015;31:261–72. https://doi.org/10.1007/S10565-015-9309-6/METRICS.
51. Jeong B, Bae YH, Lee DS, Kim SW. Biodegradable block copolymers as injectable drug-delivery systems. Nature. 1997. https://doi.org/10.1038/42218.
52. Yasugi K, Nagasaki Y, Kato M, Kataoka K. Preparation and characterization of polymer micelles from poly(ethylene glycol)-poly(d, l-lactide) block copolymers as potential drug carrier. J Control Release. 1999;62:89–100. https://doi.org/10.1016/S0168-3659(99)00028-0.
53. Shan X, Yuan Y, Liu C, Xu F, Sheng Y. Comparison of the PLA-mPEG and mPEG-PLA-mPEG copolymers nanoparticles on the plasma protein adsorption and in vivo biodistribution. Soft Matter. 2009;5:2875–83.
54. Ghasemi R, Abdollahi M, Emamgholi Zadeh E, Khodabakhshi K, Badeli A, Bagheri H, Hosseinkhani S. MPEG-PLA and PLA-PEG-PLA nanoparticles as new carriers for delivery of recombinant human Growth Hormone (rhGH). Sci Rep. 2018;8:1–13. https://doi.org/10.1038/s41598-018-28092-8.

55. Danafar H, Rostamizadeh K, Davaran S, Hamidi M. PLA-PEG-PLA copolymer-based polymersomes as nanocarriers for delivery of hydrophilic and hydrophobic drugs: preparation and evaluation with atorvastatin and lisinopril. Drug Dev Ind Pharm. 2014;40:1411–20. https://doi.org/10.3109/03639045.2013.828223.
56. Cui F, Cun D, Tao A, Yang M, Shi K, Zhao M, Guan Y. Preparation and characterization of melittin-loaded poly (DL-lactic acid) or poly (DL-lactic-co-glycolic acid) microspheres made by the double emulsion method. J Control Release. 2005;107:310–9. https://doi.org/10.1016/j.jconrel.2005.07.001.
57. Foulkes R, Man E, Thind J, Yeung S, Joy A, Hoskins C. The regulation of nanomaterials and nanomedicines for clinical application: current and future perspectives. Biomater Sci. 2020;8:4653–64. https://doi.org/10.1039/D0BM00558D.
58. Suk JS, Xu Q, Kim N, Hanes J, Ensign LM. PEGylation as a strategy for improving nanoparticle-based drug and gene delivery. Adv Drug Deliv Rev. 2016;99:28–51. https://doi.org/10.1016/J.ADDR.2015.09.012.
59. E.T. de Melo et al. 2015.pdf, (n.d.).
60. Corzo G, Escoubas P, Villegas E, Barnham KJ, He W, Norton RS, Nakajima T. Characterization of unique amphipathic antimicrobial peptides from venom of the scorpion Pandinus imperator. Biochemical Journal. 2001;359:35–45. https://doi.org/10.1042/0264-6021:3590035.
61. Zhao Z, Ma Y, Dai C, Zhao R, Li S, Wu Y. Imcroporin, a new cationic antimicrobial peptide from the venom of the scorpion isometrus maculates. Antimicrob Agents Chemother. 2009;53:3472–7. https://doi.org/10.1128/AAC.01436-08.
62. Gasu EN, Ahor HS, Borquaye LS. Peptide extract from olivancillaria hiatula exhibits broad-spectrum antibacterial activity. Biomed Res Int. 2018. https://doi.org/10.1155/2018/6010572.
63. Levison ME. Pharmacodynamics of antimicrobial drugs. Infect Dis Clin North Am. 2004;18:451–65. https://doi.org/10.1016/j.idc.2004.04.012.
64. Osorio-Alvarado CE, Ropero-Vega JL, Farfán-García AE, Flórez-Castillo JM. Immobilization systems of antimicrobial peptide Ib–M1 in polymeric nanoparticles based on alginate and chitosan. Polymers. 2022. https://doi.org/10.3390/polym14153149.
65. Lv S, Sylvestre M, Song K, Pun SH. Development of D-melittin polymeric nanoparticles for anti-cancer treatment. Biomaterials. 2021;277:121076. https://doi.org/10.1016/j.biomaterials.2021.121076.
66. van Gent ME, Ali M, Nibbering PH, Kłodzińska SN. Current advances in lipid and polymeric antimicrobial peptide delivery systems and coatings for the prevention and treatment of bacterial infections. Pharmaceutics. 2021. https://doi.org/10.3390/pharmaceutics13111840.
67. Cao J, Zhang Y, Shan Y, Wang J, Liu F, Liu H, Xing G, Lei J, Zhou J. A pH-dependent antibacterial peptide release nano-system blocks tumor growth in vivo without toxicity. Sci Rep. 2017;2017(17):1–13. https://doi.org/10.1038/s41598-017-11687-y.
68. Jiang Z, Li Y, Wei Z, Yuan B, Wang Y, Akakuru OU, Li Y, Li J, Wu A. Pressure-induced amorphous zeolitic imidazole frameworks with reduced toxicity and increased tumor accumulation improves therapeutic efficacy In vivo. Bioact Mater. 2021;6:740–8. https://doi.org/10.1016/J.BIOACTMAT.2020.08.036.
69. Derakhshan-sefidi M, Bakhshi B, Rasekhi A. Thiolated chitosan nanoparticles encapsulated nisin and selenium: antimicrobial/antibiofilm/anti-attachment/immunomodulatory multi-functional agent. BMC Microbiol. 2024. https://doi.org/10.1186/s12866-024-03400-7.
70. Milani F, Adibkia K, Hamishehkar H, Gholikhani T, Bani F, Milani M. Increased antibiofilm and growth inhibitory effect of Imipenem/Cilastatin nanoliposomes against clinical Pseudomonas aeruginosa isolates. J Mater Sci Mater Med. 2023. https://doi.org/10.1007/s10856-023-06752-0.
71. Liu S, Meng F, Guo S, Yuan M, Wang H, Chang X. Inhibition of α-amylase digestion by a Lonicera caerulea berry polyphenol starch complex revealed via multi-spectroscopic and molecular dynamics analyses. Int J Biol Macromol. 2024;260: 129573. https://doi.org/10.1016/J.IJBIOMAC.2024.129573.
72. Almaaytah A, Mohammed GK, Abualhaijaa A, Al-Balas Q. Development of novel ultrashort antimicrobial peptide nanoparticles with potent antimicrobial and antibiofilm activities against multidrug-resistant bacteria. Drug Des Devel Ther. 2017;11:3159–70. https://doi.org/10.2147/DDDT.S147450.
73. Watcharadulyarat N, Rattanatayarom M, Ruangsawasdi N, Patikarnmonthon N. PEG-PLGA nanoparticles for encapsulating ciprofloxacin. Sci Rep. 2023. https://doi.org/10.1038/s41598-023-27500-y.
74. Zhang Z, Wang L, Guo Z, Sun Y, Yan J. A pH-sensitive imidazole grafted polymeric micelles nanoplatform based on ROS amplification for ferroptosis-enhanced chemodynamic therapy. Colloids Surf B Biointerfaces. 2024;237: 113871. https://doi.org/10.1016/J.COLSURFB.2024.113871.
75. Wang Y, Xu Y, Song J, Liu X, Liu S, Yang N, Wang L, Liu Y, Zhao Y, Zhou W, Zhang Y. Tumor Cell-Targeting and Tumor Microenvironment-Responsive Nanoplatforms for the Multimodal Imaging-Guided Photodynamic/Photothermal/Chemodynamic Treatment of Cervical Cancer. Int J Nanomed. 2024;19:5837–58. https://doi.org/10.2147/IJN.S466042.